Results in Engineering 24 (2024) 103240

Contents lists available at ScienceDirect

Results in Engineering

journal homepage: www.sciencedirect.com/journal/results-in-engineering

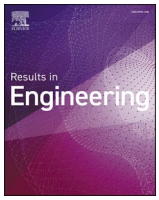

Research paper

# Numerical and experimental investigation of Darrieus vertical axis wind turbines to enhance self-starting at low wind speeds

Hossein Seifi Davari [a,*], Ruxandra Mihaela Botez [b], Mohsen Seify Davari [c], Harun Chowdhury [d], Hasan Hosseinzadeh [e]

[a] Department of Mechanical & Marine Engineering, Chabahar Maritime University, Chabahar, Iran
[b] Laboratory of Applied Research in Active Controls, Avionics, and AeroServoElasticity LARCASE, École de Technologie Supérieure, Université de Québec, Montréal, QC H3C 1K3, Canada
[c] Faculty of Engineering and Technology, Islamic Azad University, Germi, Iran
[d] School of Engineering, RMIT University, Melbourne, VIC-3000, Australia
[e] Department of Mathematics, Islamic Azad University Ardabil Branch, Ardabil, Iran

ARTICLE INFO

*Keywords:*
Rotation
DMST
NACA0015, Embossed-bladed vawt
Wind speed

ABSTRACT

Wind energy, being renewable, cost-effective, and environmentally friendly, has attracted global attention. However, due to suboptimal performance and limited research, vertical axis wind turbines (VAWTs) lag behind horizontal axis wind turbines (HAWTs) in commercial applications, particularly for large-scale installations. This study aims to improve the self-starting capability of the Darrieus VAWT. While some parameters, such as the number of blades (N) and solidity (σ), have been studied extensively, the airfoil shape has not received as much attention. This study compares the performance of National Advisory Committee for Aeronautics (NACA) airfoils and Selig airfoils at a Reynolds number (Re) of 40,673. The investigation revealed that the NACA0015 airfoil exhibited the highest peak power coefficient ($C_p$). Further analysis utilizing an advanced double multiple stream tube (DMST) code in MATLAB increased the peak $C_p$ by adjusting the thickness-to-camber ratio (t/c) of the NACA0015 airfoil, resulting in a 12.50 % increase in the maximum achievable $C_p$ at a Re of 40,673. This study compared four modes of VAWT operation, utilizing the NACA0015 airfoil and a modified NACA0015 airfoil for both straight-bladed and embossed-bladed VAWTs. The results showed that the modified NACA0015 airfoil for embossed-bladed VAWTs exhibited the best self-starting capability and rotation at wind velocities of 1 to 9 m $s^{-1}$. Additionally, the self-starting force required by embossed-bladed VAWTs was lower than that needed by straight-bladed VAWTs due to the ability of the embossed material to enhance airflow attachment to the VAWT and suppress turbulence.

## 1. Introduction

Although fossil fuels are still plentiful, their use results in substantial carbon dioxide emissions and other harmful pollutants, contributing to global warming and degrading air quality [1–7]. This underscores the necessity for sustainable alternatives [8–10]. Renewable energy sources, including solar, wind, and hydropower, provide viable solutions to these environmental challenges [11–22].

Among these, wind energy stands out for its high efficiency and minimal environmental impact [23–25]. This study focuses on wind energy, specifically exploring the functionality and benefits of wind turbines (WTs). WTs convert kinetic energy from the wind into electrical power, providing a clean and renewable energy source [26–28]. They can be broadly classified into two types based on the orientation of their axes: HAWTs and VAWTs [29–31].

HAWTs are the most common type, characterized by a rotor shaft and electrical generator positioned at the top of a tower, with blades rotating on a horizontal axis [32,33]. These turbines must be aligned with the wind direction, which can be achieved through a small wind vane or a more sophisticated sensor and servo motor system [34,35]. One of the main advantages of HAWTs is their higher efficiency compared to VAWTs, as they can harness more wind energy [36,37]. However, HAWTs also have disadvantages, including the need for a mechanism to orient the blades into the wind, which adds complexity and cost [38,39].

* Corresponding author.
*E-mail address:* hseifidavary@gmail.com (H. Seifi Davari).

https://doi.org/10.1016/j.rineng.2024.103240
Received 30 August 2024; Received in revised form 20 October 2024; Accepted 23 October 2024
Available online 29 October 2024

**Nomenclature**

| Acronym | Full Form |
|---|---|
| AoA | Angle of Attack (Deg) |
| AR | Aspect Ratio (-) |
| C | Chord length (cm) |
| $C_D$ | Drag coefficient (-) |
| $C_L$ | Lift coefficient (-) |
| $C_N$ | Normal coefficient (-) |
| $C_p$ | Power coefficient (-) |
| $C_T$ | Tangential coefficient (-) |
| CFD | computational fluid dynamics |
| D | Diameter of rotor (cm) |
| DMST | Double Multiple Stream Tube |
| GF | Gurney Flap |
| H | Height of rotor (cm) |
| HAWT | Horizontal Axis Wind Turbine |
| L/D | Lift-to-drag ratio (-) |
| LWS | Low Wind Speed |
| N | Number of blades (-) |
| NACA | National Advisory Committee for Aeronautics |
| R | The radius of the rotor (cm) |
| Re | Reynolds number (-) |
| t/c | Thickness-to-camber ratio (-) |
| TSR | Tip Speed Ratio |
| $V_\infty$ | Wind speed (m $s^{-1}$) |
| VAWT | Vertical Axis Wind Turbine |
| WT | Wind Turbine |
| ɑ | Axial induction factor |
| a′ | Tangential induction factor |
| ß | pitch angle (Deg) |
| $\rho$ | Air density (Kg/$m^3$) |
| $\mu$ | Dynamic viscosity (Kg $m^{-1}s^{-1}$) |
| $\upsilon$ | Kinematic viscosity ($m^2s^{-1}$) |
| $\omega$ | Angular speed (rad $s^{-1}$) |
| Θ | The azimuth angle |
| σ | Solidity (-) |

Among the VAWTs, the Darrieus and Savonius designs are the most notable. These two types have distinct operational principles and performance characteristics. The Savonius VAWT operates on the principle of aerodynamic drag, generally consisting of two or more scoops that catch the wind, causing the rotor to turn. Its simple and robust design makes it effective at low wind speeds (LWSs). However, reliance on drag results in lower efficiency compared to lift-based systems, as the wind's impact on the scoops produces less torque [40–43].

In contrast, the Darrieus VAWT operates based on the principle of aerodynamic lift. The lift force on its blades creates rotational motion that drives the VAWT. This design is known for its high efficiency, as it can achieve greater rotational speeds and convert wind energy into mechanical energy more effectively than drag-based systems [44,45]. One of the main disadvantages of the Darrieus VAWT is its characteristic of being "non-self-starting." To understand this limitation, it is essential to define and explain the concept of self-starting in WTs. Self-starting refers to a WT's ability to rotate and generate power from a stationary position without external assistance. For a VAWT to have self-starting capability, it must capture enough wind force at low LWSs to overcome inertia and start turning on its own. Darrieus VAWTs typically lack this capability [46–48].

The theoretical maximum efficiency of Darrieus VAWTs is about 35 %, higher than the roughly 12–15 % efficiency of cross-flow wind turbines but lower compared to HAWTs, which can achieve efficiencies of up to 45 % [49]. Recent studies indicate that VAWTs may outperform HAWTs in urban and semi-urban environments. Research highlights several advantages of VAWTs in these areas, including lower costs, reduced noise and vibration, resistance to changes in wind direction, and minimal visual disruption. These attributes enhance public safety and aesthetics, making VAWTs more appealing for installation in locations where conventional HAWTs may be less effective or appropriate [49]. However, given the challenges of self-starting and the relatively lower efficiency of VAWTs compared to HAWTs, numerous studies have been conducted to improve the efficiency and self-starting capabilities of VAWTs.

In WTs, design and other factors are essential. Research by Sunny et al. [50] focused on using curved blades to develop small-scale VAWTs. Wind tunnel experiments were conducted, and the results were reported for VAWTs with two-blade, three-blade, and four-blade configurations. Their findings indicated that the curved blade WT with a three-blade setup outperformed the other two configurations. A variable pitch system can significantly enhance the efficiency of vertical axis turbines, resulting in a 35 % increase in efficiency and reducing unsteady loads on the VAWT [51]. However, implementing a variable pitch system also introduces several disadvantages. The complexity and cost of the system are significant drawbacks. Additionally, the increase in moving parts necessitates frequent maintenance and inspections, leading to higher operational costs and potential downtime [52].

A Darrieus VAWT with symmetric airfoils, as well as a Darrieus-Savonius VAWT, was also examined. The Darrieus VAWT exhibited no self-starting capabilities at wind speeds ($V_\infty$) below 3.65 m $s^{-1}$. In contrast, a proposed hybrid Darrieus-Savonius WT had a self-starting velocity down to 2.81 m $s^{-1}$ and achieved a power output of 1.522 kW at a $V_\infty$ of 7.5 m $s^{-1}$ [53]. Overall, combining Darrieus and Savonius VAWTs enhances self-starting capabilities but reduces peak performance [54]. Cheng and Yao [55] analyzed a novel U-type Darrieus VAWT. Their results showed that the optimal U-type Darrieus VAWT can operate successfully, with the $C_p$ increased by 14.74 % and by 54 % at tip speed ratios (TSRs) of 4.0 and 4.5, respectively. Other research indicated that the V-shaped blade efficiently mitigated flow separation [56].

A significant drawback of U-type Darrieus and V-shaped VAWTs is their complex design and manufacturing processes, which make them expensive. While the J-shaped Darrieus VAWT showed better performance than the V-shaped Darrieus VAWTs during self-starting conditions and at low TSRs, the total torque decreased at TSRs above 2.25 due to the lower lift coefficient ($C_L$) of the J-shaped blades [57]. In another effort to enhance the efficiency of VAWTs, the Gurney flap (GF) significantly improved the aerodynamic performance of VAWTs at reduced rotational velocities. In the upstream area, the GF notably increased the tangential force on the blades [58]. However, installing GFs added complexity to the VAWT design, increasing manufacturing costs and maintenance needs.

To enhance the self-starting capability of the Darrieus VAWT, a conical wind collector was attached, resulting in a 25 % improvement in its self-starting performance [59]. It should be noted that the installation of the wind collector generally increased the radius (R) and height (H) of the VAWT. The study conducted by Celik et al. [60] showed that increasing the inertia of the VAWT did not significantly affect its self-starting capacity. Sun et al. [61] demonstrated that turbulence increases fatigue issues in helical VAWTs and impacts their operational mechanism, even though it improves their self-starting capability.

To lower the manufacturing and installation costs of the Darrieus VAWT while maintaining balance, this study employed a three-blade design [62,63]. Due to cyclical variations in the angle of attack (AoA) and operation at different AoAs, the VAWT blades can experience

dynamic stall at low TSRs [64–68]. This situation complicates the design of an optimal airfoil [69]. Additionally, a significant challenge with Darrieus VAWT rotors is the negative torque coefficient observed at low TSRs. A flexible VAWT design enhances lift and torque, particularly in downstream areas, by effectively managing blade-wake interactions and optimizing the blade AoA, thereby improving overall VAWT performance. However, the complexity of these mechanisms and the need for structural stability present significant challenges to implementing this approach [70].

Karmakar and Chattopadhyay [71] illustrated that integrating enhancement devices such as deflectors, guide vanes, converging ducts, diffusers, and stators with VAWTs created a venturi effect at the inlet. This effect improved positive torque and boosted the self-starting ability of VAWTs. However, these systems introduced certain drawbacks, including increased complexity in design, higher manufacturing and maintenance costs, and potential inefficiencies under specific operational conditions. Additionally, controlling the pitch angle (β) of the entire blade required a complex four-bar linkage system, leading to higher maintenance and operational costs [72].

Rajpar et al. [73] reviewed several studies and found that using wind deflectors to enhance airflow not only reduced the negative torque generated by the retreating blades but also increased the positive torque by directing upstream wind toward the advancing blades during operation. However, wind deflectors also presented disadvantages, such as potential increases in overall turbine weight, added complexity in system design, and possible aerodynamic interference that could affect the turbine's performance under certain conditions.

Several computational models are used to assess the efficiency of VAWTs. Wind tunnel studies [74–76] and numerical studies using the computational fluid dynamics (CFD) approach [77,78] evaluate the aerodynamic efficiency of turbines. Momentum models, such as stream tube models, are effective tools for efficiency investigations. Results obtained from these models align well with both wind tunnel results [79] and CFD results [80]. The rapid prediction capability and performance of the DMST model have demonstrated its reliability in determining the dynamics of VAWTs [81–84].

The selection of airfoils for VAWTs is a crucial factor influencing energy costs and aerodynamic performance, representing a significant opportunity for innovation in wind energy technology. Choosing the right airfoil design is essential for maximizing aerodynamic efficiency and maintaining the structural integrity of the blades. The dynamic nature of VAWTs, characterized by continuous changes in AoA and differential speeds, necessitates the use of specifically designed airfoils. This is especially true when considering the influence of *Re* on the aerodynamic behavior of small-scale WTs. The importance of *Re* cannot be overstated; it serves as a fundamental parameter that dictates the flow characteristics around the blades. For small-scale VAWTs operating at low *Re*, selecting an appropriate airfoil is paramount for achieving reliable and accurate performance data. Emphasizing innovation in airfoil selection for these turbines is crucial for enhancing their effectiveness and reliability. This approach will ultimately contribute to the development of more efficient wind energy systems, reinforcing the significance of airfoil design in the quest for sustainable energy solutions.

Moreover, the present study extends beyond the current state-of-the-art in the field of VAWTs by introducing and experimentally investigating a novel blade design—embossed-bladed Darrieus VAWTs. While most recent studies have focused on conventional straight-bladed designs or hybrid configurations, such as Darrieus-Savonius models, none have considered the potential advantages of embossed blade geometries in improving self-starting capabilities. The unique embossed design is expected to alter the aerodynamic profile of the blades, enhancing the lift-to-drag ratio (L/D) at low TSRs and facilitating a smoother and more efficient self-starting mechanism, particularly in LWS conditions, which is a significant drawback of traditional Darrieus VAWTs.

In addition to the embossed blades, this study further examines modified airfoils alongside the embossed blades. This experimental comparison evaluates the performance of embossed-bladed VAWTs against straight-bladed VAWTs and baseline airfoils. Previous research has primarily focused on numerical and wind tunnel studies, employing conventional methods such as CFD and simplified stream tube models. In contrast, this study utilizes an advanced and customized DMST model to investigate the performance of the embossed-bladed VAWTs compared to straight-bladed VAWTs and modified airfoils. This approach allows the research to provide new insights into how geometric modifications directly influence both the aerodynamic $C_p$ and self-starting torque—areas that have not been comprehensively addressed in the literature.

Thus, this study not only addresses a significant gap by exploring embossed-bladed and modified airfoil VAWTs but also advances the state of the art by providing experimental data on self-starting performance. This data can contribute to the design of more efficient and reliable VAWTs for practical applications, especially in regions with LWSs. These innovations offer substantial improvements over traditional designs, effectively tackling longstanding challenges in the field.

## 2. DMST model

In the DMST model, the rotor area is divided into upstream and downstream sections, as illustrated in Fig. 1, where air moves through actuator disks within a tube.

The flow conditions for each stream tube are evaluated by combining momentum theory with blade element theory. Momentum theory is based on the conservation of angular and linear momentum, while blade element theory analyzes the forces on the blades by dividing them into finite elements based on their shapes. In the DMST model, instead of segmenting the blade, the entire turbine circumference is divided into a finite number of stream tubes. As shown in Fig. 1, V, V′, and $V_\infty$ denote the local upwind speed ($\frac{-\pi}{2} < \Theta < \frac{\pi}{2}$), downwind speed ($\frac{\pi}{2} < \Theta < \frac{3\pi}{2}$), and $V_\infty$, respectively. These speeds can be calculated using the following equations [86,87]:

$$V = aV_\infty \tag{1}$$

$$V_e = (2a-1)V_\infty \tag{2}$$

$$V' = a'(2a-1)V_\infty \tag{3}$$

where $V_e$ equals the speed in the joining area of both semi-tubes. The a′ and ɑ represent the tangential induction and axial induction factors, respectively. The local relative wind velocity encountered by the blade is influenced by the local TSR, and the induced speed [86,87]:

$$w = V_\infty\sqrt{(TSR + a\sin(\theta))^2 + (a\cos(\theta))^2} \tag{4}$$

where w represents the relative speed, Θ denotes the azimuth angle, and TSR refers to the local TSR as obtained by Islam et al. [86]:

$$TSR = \frac{R\omega}{V_\infty} \tag{5}$$

where $\omega$ represents the rotational speed. The tangential coefficient ($C_T$), drag coefficient ($C_D$), and normal coefficient ($C_N$) can be computed utilizing the following equations [86]:

$$C_N = C_L\cos(\alpha) + C_D\sin(\alpha) \tag{6}$$

$$C_T = C_L\sin(\alpha) - C_D\cos(\alpha)$$

The AoA is also obtained [85].

$$AoA = \tan^{-1}\left(\frac{a\cos(\theta)}{TSR + a\sin(\theta)}\right) \tag{7}$$

By integrating momentum with blade element theory for each stream

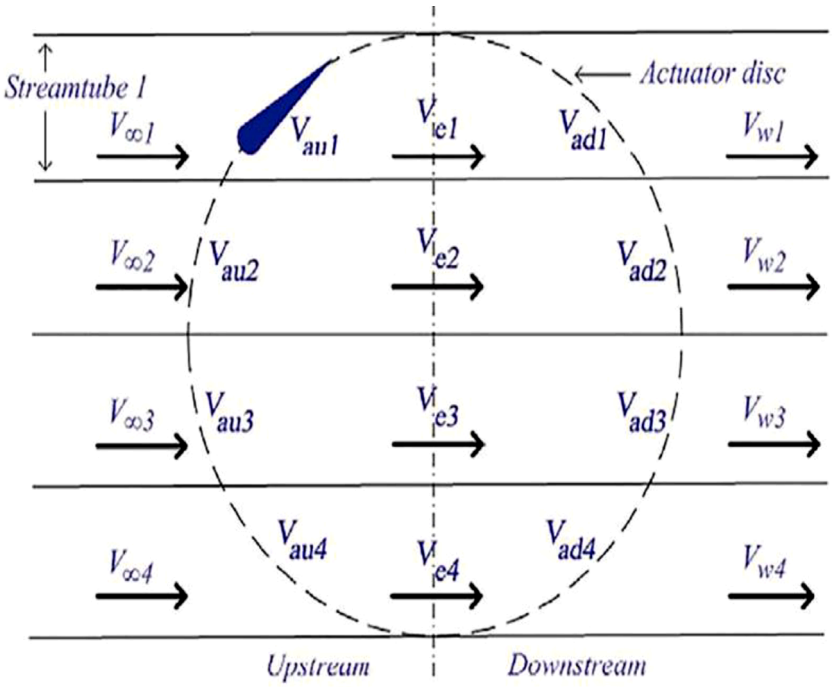


**Fig. 1.** The DMST model diagram [85].

tube [86], the value of a is provided by Batista et al. [85] and Paraschivoiu [87]:

$$a = \frac{\pi}{F_{up} + \pi} \tag{8}$$

where $F_{up}$ is defined by Islam [86] and Paraschivoiu [87]:

$$F_{up} = \frac{\sigma}{2\pi} \int_{-\frac{\pi}{2}}^{\frac{\pi}{2}} \left(\frac{w}{V_\infty}\right)^2 \times \left(C_N \frac{\cos(\theta)}{|\cos(\theta)|} - C_T \frac{\sin(\theta)}{|\cos(\theta)|}\right) d\theta \tag{9}$$

where$\sigma$represents solidly.

$$\sigma = \frac{NC}{D} \tag{10}$$

This relationship depends on the chord length (C) and the rotor diameter (D). The $C_p$ for the upwind section is calculated according to Batista et al. [85], as follows:

$$C_{Pup} = \frac{TSR \times \sigma}{4\pi} \int_{-\frac{\pi}{2}}^{\frac{\pi}{2}} C_T \left(\frac{w}{V_\infty}\right)^2 d\theta \tag{11}$$

The identical equations are applied for the downwind section using ($V_e$) instead of (V), as specified in Eq. (3). The overall $C_p$ is computed for one cycle as follows:

$$C_P = C_{Pup} + C_{Pdw} \tag{12}$$

A DMST code was developed in this study, and its methodology is illustrated in the flowchart shown in Fig. 2.

Subsequently, as mentioned earlier, the VAWT area is divided into two regions: the upwind and downwind regions. An initial value is assumed for the a, and then Eqs. (4) to (9) are iteratively solved to find a new value for a. If the difference between the computed and assumed values of a exceeds a specified threshold, the process continues until convergence is achieved. This iterative process is then applied to the downwind section, using the computed value of a as the initial amount for a′. After computing the amounts of a and a′, the $C_p$ of the WT is computed utilizing Eqs. (11) and (12).

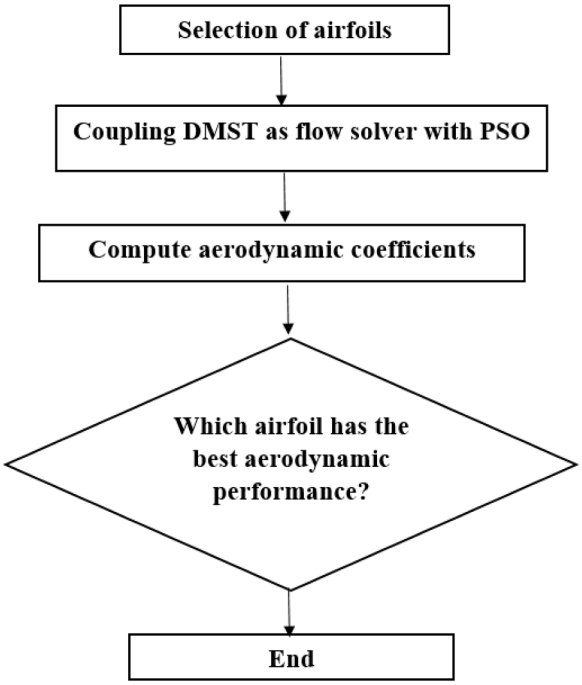


**Fig. 2.** Outline of the employed methodology.

Additionally, other data from the literature were used to validate the results of the DMST code in MATLAB. The experimental results from Elkhoury et al.'s [88] study on a Darrieus VAWT and the DMST model developed by Ghiasi et al. [87] were utilized for validation. They conducted numerical and experimental investigations on the efficiency of a VAWT with a length of 80 cm, and $D = 80$ cm. Their VAWTs featured a symmetrical blade profile (NACA0018) with C = 20 cm. The validation of our DMST code results was performed at TSR values ranging from 0 to 3, and these results were compared with the experimental data obtained

by Elkhoury et al. [88].

Fig. 3 compares the DMST code developed in MATLAB in this work with the experimental from [88] and simulation results of a DMST model [87]. This comparison indicates a relatively good agreement between the estimated and experimental results. Assuming constant speed, frontal area, and air density (ρ), the relationship between the $C_p$ and TSR remains consistent. The maximum difference between experimental and DMST results occurred at a TSR of 1, with a difference of 4.2 %.

## 3. Airfoil properties

The maximum $C_p$ value for forty-four VAWT rotors, including symmetrical and unsymmetrical NACA 4-digit, 5-digit, 6-digit, and Selig airfoils, was determined at a chord *Re* of 40,673 using the developed DMST method. The ρ is approximately 1.184 kg $m^{-13}$, the C is 0.71 cm, and the dynamic viscosity of air is 0.0000186 kg/(m·s). The inlet $V_\infty$ is assumed to be 9 m $s^{-1}$. Additionally, the chord *Re* was calculated using Eq. (13).

$$\mathrm{Re}_c = \frac{\rho V_\infty C}{\mu} \tag{13}$$

Table 1 shows the maximum $C_p$ values for all rotors tested at a chord *Re* of 40,673 and a TSR of 2. The NACA0015 rotor airfoil achieved the highest maximum $C_p$ value of 0.152, outperforming all 43 others. The simulation was conducted at TSR values ranging from 0 to 3, in increments of 0.50.

Other studies have shown that among symmetrical airfoil designs, the NACA 0015 is especially advantageous for aerodynamic performance. It minimizes the rotor's inactive zone at very low TSR and provides a higher average $C_p$ distribution across the full range of TSR values [89,90].

### 3.1. Modified airfoil shape

The initial purpose of the optimization procedure was to alter the airfoil's geometry to enhance its aerodynamic performance. The method for optimizing this airfoil is summarized in Fig. 4. As stated earlier, this study yielded the highest $C_p$ with t/c at a Re of 40,673 due to the optimization results for the NACA0015 airfoil. As shown graphically in Fig. 5, the NACA0015 was optimized to have a peak thickness of 14.54 % at C = 31.10 % and a peak camber of 1.13 % at C = 46.70 %. The thickness and camber of the airfoils' geometric features were the primary differences between the NACA0015 and the developed NACA0015-Mod airfoils.

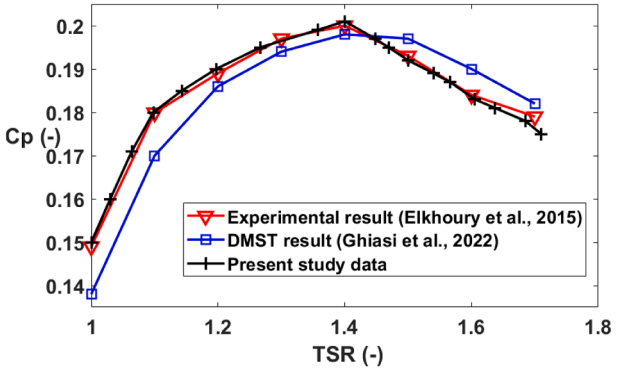


**Fig. 3.** Validation data of developed DMST code with experimental and DMST data.

**Table 1**
The maximum $C_P$ values for selected rotors at a *Re* value of 40,673 with a TSR of 2.

| Airfoil types | TSR | Maximum $C_P$ |
|---|---|---|
| NACA0010 | 2 | 0.148 |
| NACA0015 | 2 | 0.152 |
| NACA0016 | 2 | 0.145 |
| NACA0018 | 2 | 0.089 |
| NACA0020 | 2 | 0.037 |
| NACA0021 | 2 | −0.003 |
| NACA0022 | 2 | −0.002 |
| NACA0030 | 2 | −0.18 |
| NACA3515 | 2 | −0.04 |
| NACA3523 | 2 | −0.087 |
| NACA3525 | 2 | −0.09 |
| NACA3528 | 2 | −0.13 |
| NACA3535 | 2 | −0.15 |
| NACA6318 | 2 | 0.10 |
| NACA6520 | 2 | 0.008 |
| NACA6525 | 2 | −0.144 |
| NACA23010 | 2 | 0.142 |
| NACA23030 | 2 | −0.093 |
| NACA24010 | 2 | 0.12 |
| NACA63(3)−618 | 2 | −0.002 |
| NACA63(4)−221 | 2 | 0.048 |
| NACA63(4)−421 | 2 | −0.023 |
| NACA64(1)−112 | 2 | 0.104 |
| NACA64(2)−215 | 2 | 0.089 |
| NACA64(4)−221 | 2 | −0.054 |
| NACA65(1)−212 | 2 | 0.084 |
| NACA65(2)−215 | 2 | 0.072 |
| NACA65(2)−415 | 2 | 0.077 |
| NACA65(3)−218 | 2 | 0.006 |
| NACA65(4)−221 | 2 | −0.049 |
| NACA65(4)−421 | 2 | −0.043 |
| NACA66(1)−212 | 2 | 0.078 |
| NACA66(2)−215 | 2 | 0.049 |
| NACA66(3)−218 | 2 | 0.027 |
| NACA66(4)−221 | 2 | 0.006 |
| S814 | 2 | 0.102 |
| S815 | 2 | 0.056 |
| S818 | 2 | 0.009 |
| S821 | 2 | 0.009 |
| S823 | 2 | −0.054 |
| S828 | 2 | 0.129 |
| S835 | 2 | −0.033 |
| S1020 | 2 | 0.021 |
| S1046 | 2 | 0.084 |

## 4. Small vawt model design and fabrication

Smooth or solid blades, known as straight blades, have been experimentally studied for decades [91–97] in investigations related to self-starting VAWTs. This research utilized an embossed-bladed VAWT and compared its self-starting performance with that of straight-bladed VAWTs. An embossed sheet was applied to the VAWT blades to enhance porosity. Diamond-embossed aluminum sheeting features a textured surface resembling crocodile skin. This texture provides a regular embossed pattern that increases friction and prevents sliding.

The sheets are made from lightweight metal stock, with a pattern of raised diamonds or lines on one side. These aluminum sheets, characterized by their diamond-embossed pattern, are homogeneous, isotropic, and environmentally friendly, making them easily recyclable. A computer numerical control laser cutting machine was used to ensure precise shapes of the sheets. Fig. 6 depicts 0.03 cm-thick straight (a) and embossed (b) aluminum blades that cover portions of the WT blades.

To ensure structural stability, an aluminum pole with a circular cross-section was selected for the shaft, with each blade attached at a distance of 8.75 cm. A central shaft made of a 2 cm-diameter iron tube was used for the VAWT. Additionally, six iron tubes with a $R = 2$ cm were chosen to attach each of the six blades to the shaft.

Fig. 7 and Table 2 illustrate the blade geometry and present a three-

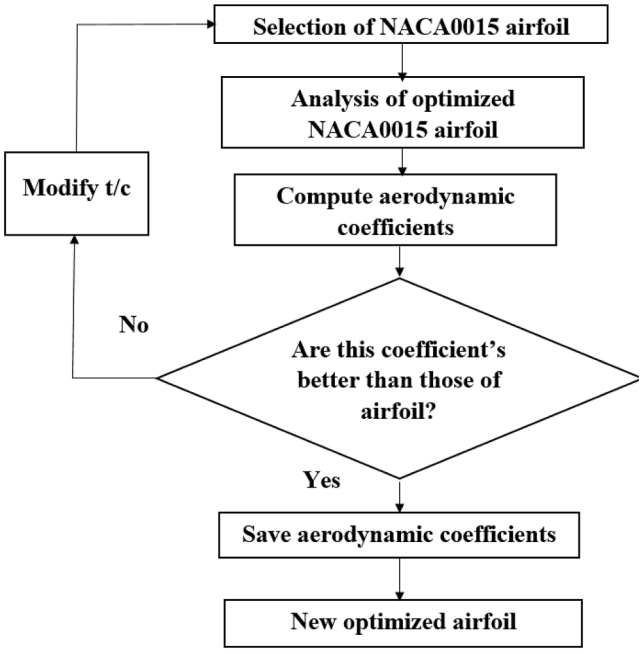


**Fig. 4.** Flowchart for developing an optimized airfoil.

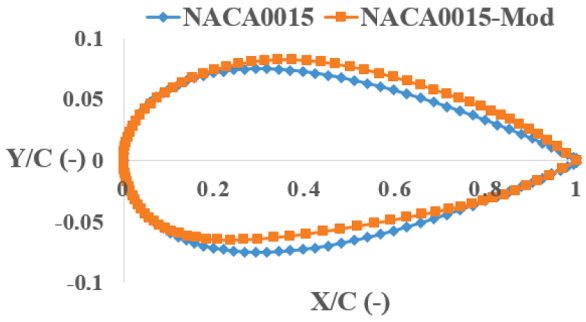


**Fig. 5.** Comparison between the NACA0015 airfoil and its optimized shape.

dimensional view of the VAWT. The aspect ratio (AR), a critical parameter that significantly affects VAWT performance, was set to 1 for this Darrieus VAWT. This AR is optimal as it provides the highest TSR and maximizes performance for small VAWTs [98].

Increasing the blade chord is one of the simplest methods to enhance low starting torque, which is crucial for micro VAWTs, as the force-to-friction ratio is often insufficient for rapid self-starting. To achieve a high σ value, the C was set to 0.071 m [99]. The arms were attached to the shaft using shielded metal arc welding, selected for its superior surface finish, adhesion, and cost-effectiveness [100]. Fig. 8 illustrates the VAWT assembly.

Next, the speed of the VAWT fans needs to be controlled and optimized. A dimmer switch was installed between the power source and the fans to adjust their speed. The range of $V_\infty$ was set between 0.5 and 11 m $s^{-1}$. The VAWTs were positioned close to the center of the experimental setup to minimize boundary layer disturbances. An anemometer measured the $V_\infty$ produced by the blower, with a high-quality device providing accurate readings within approximately ±0.5 m $s^{-1}$.

A force gauge was used to measure the force required for self-starting, with an accuracy of ±2 %, while a tachometer monitored the rotor's rotation, offering typical measurement accuracy of ±0.5 %. Laboratory temperature was recorded using a digital thermometer with a precision of 0.1 °C. The laboratory temperature was maintained at 21.4 °C by an air conditioner during testing, with fluctuations not exceeding 1.7 °C, making any temperature effects on measurement variations negligible. The laboratory ρ was 1.20 kg $m^{-13}$.

(a) Straight sheet

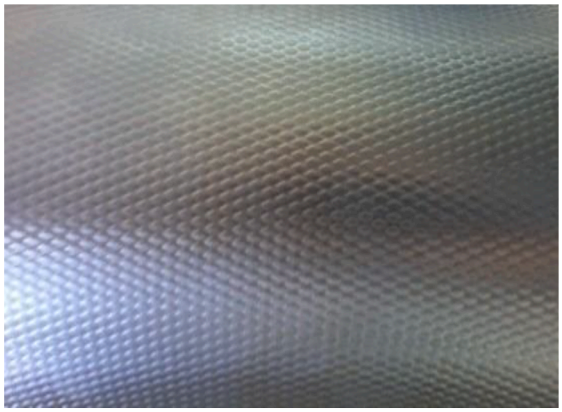

(b) Embossed sheet

**Fig. 6.** Aluminum sheets: a) straight and b) embossed bladed.

Finally, the schematic diagram of the experimental system is shown in Fig. 9(a). For the VAWT tests, a blower with four fans was used to simulate field conditions for $V_\infty$, as shown in Fig. 9(b). Four scenarios, detailed in Table 3, were investigated to evaluate the planned VAWT using the NACA0015 airfoil.

The central shaft was secured at two points using a bearing system designed to prevent vibration. During the revolutions of the VAWT, four 25-kg iron plates were employed to maintain stability.

## 5. Results and discussion

### 5.1. Aerodynamic efficiency of a VAWT

Fig. 10 displays the variation of $C_p$ with TSR for the NACA0015 and NACA0015-Mod rotors at a Re of 40,673. The simulation was conducted over a TSR range of 0 to 2.5, with increments of 0.5. The results indicate that the NACA0015-Mod rotor achieves a maximum $C_p$ value of 0.171, surpassing the maximum $C_p$ value of 0.152 for the NACA0015 rotor, representing an improvement of approximately 12.50 %. This substantial enhancement underscores the effectiveness of the design modifications made in the NACA0015-Mod rotor.

In comparison, Zhang et al. [101] investigated the impact of a bionic airfoil on the aerodynamic characteristics of a VAWT. They reported a $C_p$ increase of 7.02 % at TSR 1.38, 7.35 % at TSR 2.19, and 3.42 % at TSR 2.58. While these improvements are significant, they do not match the performance gains achieved with the NACA 0015-Mod rotor, which consistently outperforms these enhancements across a broader range of TSR.

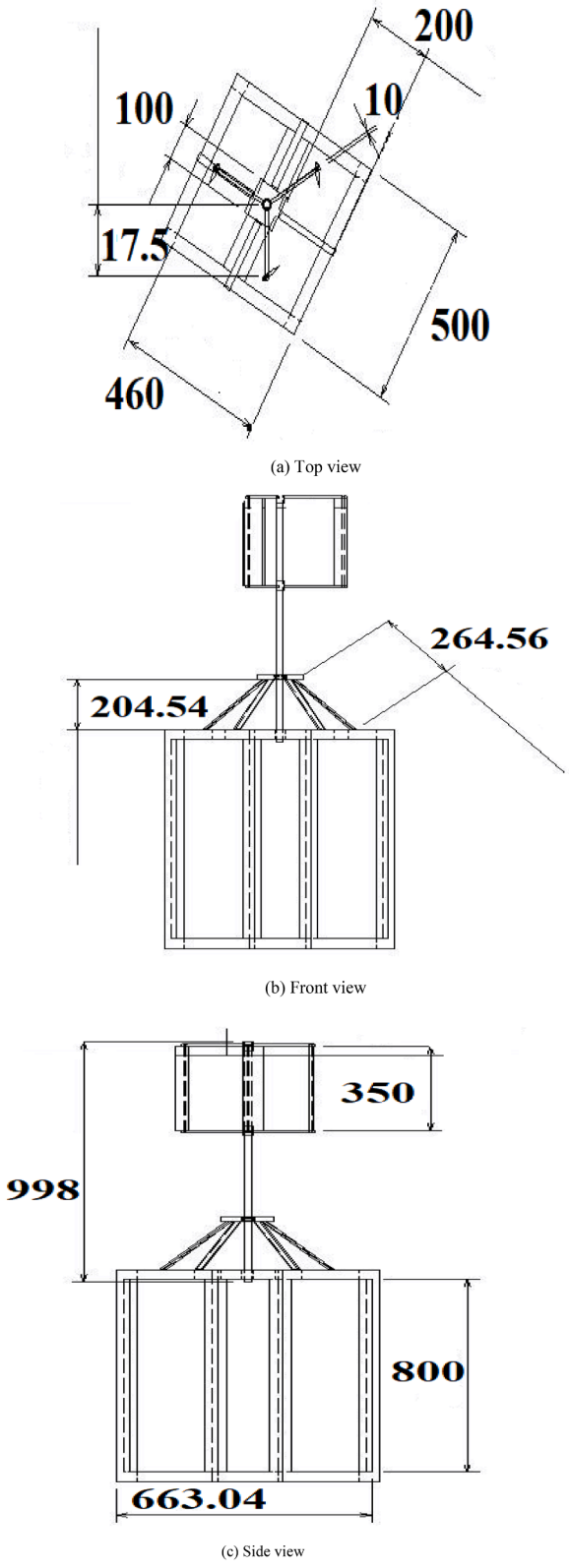


**Fig. 7.** Blade geometry (CAD drawing) from three views: (a) top, (b) front, and (c) side.

Moreover, Abul-Ela et al. [102] conducted a comprehensive study on various low Re airfoils designed for small-scale Darrieus VAWTs. Their analysis included airfoil models such as NACA0021, NACA6712, and Eppler474, revealing a maximum $C_p$ of approximately 0.3263 for the NACA0021 at a TSR of 2.63. However, the NACA0015-Mod rotor demonstrates a more substantial improvement in $C_p$ at lower TSRs, indicating its suitability for a wider range of operational conditions.

**Table 2**
Geometrical parameters of the VAWT scheme.

| Parameter | Value |
|---|---|
| R | 17.50 cm |
| H | 35 cm |
| C | 7.10 cm |
| σ | 1.15 |
| AR | 1 |
| N | 3 |
| Shaft diameter | 20 cm |
| Number of arms | 6 |
| Twist angle | 0° |

Other studies have demonstrated the effectiveness of specific design features in enhancing aerodynamic performance. For instance, research indicated that blades equipped with negatively cambered airfoil designs produced an average torque that was 8.8 % higher [103]. Additionally, incorporating a circular dimple on the pressure surface of the blades resulted in a 5.18 % increase in $C_p$ at a TSR of 2.7 compared to smooth airfoils. While these modifications are effective, they do not reach the performance levels of the NACA0015-Mod rotor [104].

Kord and Bazarghan [105] performed a numerical analysis of J-shaped, straight-bladed Darrieus VAWTs, concluding that an optimal inboard configuration enhanced power generation by 12.35 % compared to previous configurations at elevated TSRs. While this is impressive, the consistent performance improvements of the NACA0015-Mod rotor design at various TSRs illustrate its superiority in aerodynamic efficiency. Additionally, other notable findings include a 7 % increase in $C_p$ attributed to the leading-edge serration method [106] and a 10.5 % improvement in $C_p$ from extending the blade lengths from 4.00 to 4.48 times the C [107]. Although these methods show promise, the improvements of the NACA0015-Mod rotor are more significant across the operational range, emphasizing the importance of innovative design in maximizing rotor performance.

Research also indicates that the implementation of auxiliary Darrieus VAWTs can achieve a maximum $C_p$ that is approximately 5 % greater than that of traditional rotors [108]. Similarly, a study demonstrated that blades with a single surface roughness had an average L/D that is 11 % greater than that of smooth blades at all AoAs [109]. However, these findings do not match the performance levels of the NACA0015-Mod rotor.

The development of VAWTs with variable swept area blades has demonstrated improved torque and power output, achieving a maximum torque coefficient of 0.3 [110]. Nevertheless, the consistent performance gains shown by the NACA0015-Mod rotor across multiple TSRs indicate a clear advantage over these approaches. Moreover, the introduction of a porous deflector resulted in an approximately 10 % increase in maximum $C_p$ at a TSR of 1 [111].

Additionally, Somoano and Huera-Huarte [112] found that blades with a semi-flexible trailing edge can broaden the rotor's operating range, resulting in an approximately 10 % performance improvement for the VAWT. Inclusion of gusts during the steady-state period enhanced the $C_p$ of the helical VAWT by 1.97 % compared to steady conditions [113].

The development of a new vented airfoil was investigated with the aim of improving the performance of lift-driven VAWTs at low TSRs while maintaining efficiency at higher TSRs. Results indicated that this configuration achieved a 20 % increase in torque generation at low TSRs, resulting in only a slight decrease in $C_p$—up to 9 % at a TSR of 2 and approximately 1 % at higher TSRs [114]. Furthermore, blades with long-wavelength protuberances improved performance, achieving a 6.28 % increase in $C_p$ for blades with three continuous bumps [115]. The findings of MacPhee and Beyene [116] indicated that flexible rotors are more efficient than standard rigid rotors, achieving efficiency

(a) Assembled CAD model

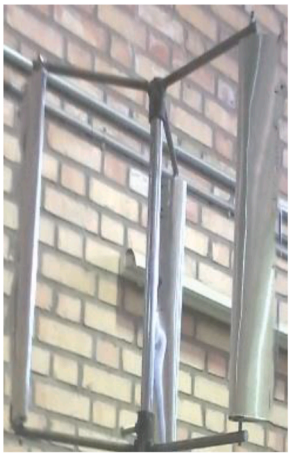

(b) Assembled straight-bladed VAWT

(c) Assembled embossed-bladed VAWT

**Fig. 8.** Assembled: (a) CAD model, (b) straight-bladed VAWT, and (c) embossed-bladed VAWT.

improvements of up to 9.6 % for the VAWT geometry studied. Guo et al. [117] investigated a hybrid rotor that combines a Φ-shaped rotor with a straight-bladed Darrieus VAWT, achieving a peak $C_p$ of 0.02531 for the hybrid rotor.

Lastly, the simulations revealed an 8 % decrease in drag for blades

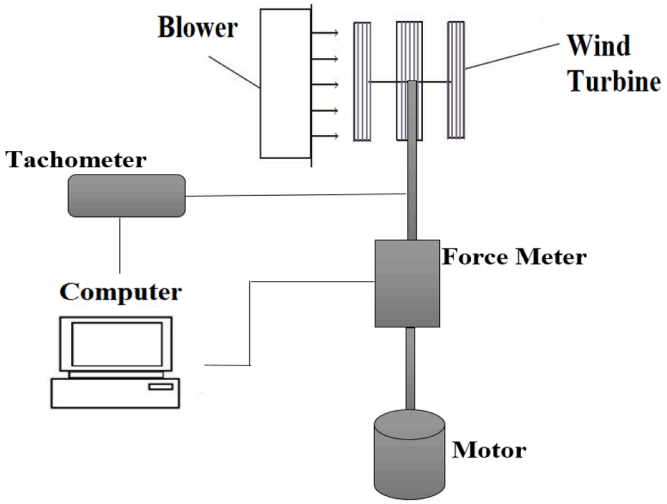


(a) Schematic turbine

(b) Test turbine

**Fig. 9.** Experimental setup: (a) schematic and (b) the test turbine.

**Table 3**
The four scenarios examined in this study.

| Scenario | |
|---|---|
| 1 | The NACA0015 airfoil for straight-bladed VAWT |
| 2 | The NACA0015 airfoil for embossed-bladed VAWT |
| 3 | The NACA0015-Mod airfoil for straight-bladed VAWT |
| 4 | The NACA0015-Mod airfoil for embossed-bladed VAWT |

equipped with slit GFs at a TSR of 2.64; however, these slit GFs also led to a 2 % reduction in $C_L$ compared to blades with standard GFs. This resulted in improved L/D and moment coefficient values. Power output also increased by 1.5 %, 6.5 %, and 11.3 % at TSRs of 1.44, 2.64, and 3.3, respectively, for the examined slit GF blades [118].

Overall, the findings from this study demonstrate that the NACA0015-Mod rotor significantly enhances aerodynamic performance, outperforming various alternative designs and methodologies found in recent studies. The consistent improvements in $C_p$ across varying TSRs highlight the effectiveness of design modifications in optimizing VAWT efficiency, representing a significant advancement in rotor design methodologies.

### 5.2. Types of experimental errors

The following experimental errors were identified in this research:

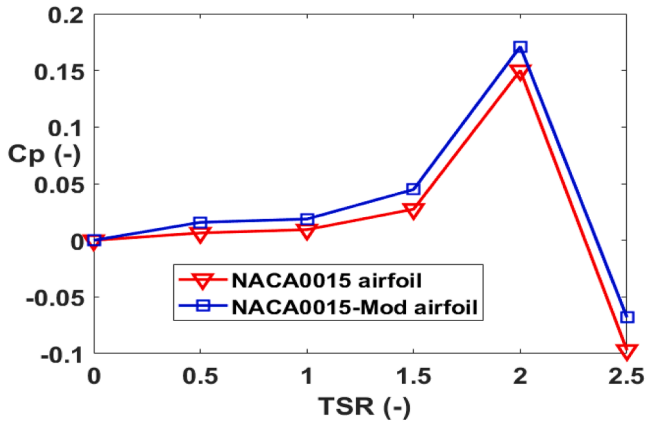


**Fig. 10.** The $C_p$ variation with TSR for the NACA0015 and NACA0015-Mod rotors at a Re = 40,673.

1. During the wind tests, $V_\infty$ was calculated using an anemometer and sensor; however, potential measurement errors may have occurred due to calibration issues or environmental factors.
2. A manual process was employed to accurately position the VAWT model for different test configurations, utilizing an indicator clock, a template, and a digital level. However, there may have been errors in adjusting distances due to human error and accuracy limitations.
3. The construction of the VAWT model could have introduced inaccuracies, such as misalignment or structural inconsistencies, that might affect the test results.
4. Although the measurement devices were well-calibrated, errors in data recording may have arisen from the 0.2 % accuracy levels of the force meter, tachometer, or anemometer.

### 5.3. *Self-starting capability at LWS*

The effectiveness of VAWTs is significantly influenced by their ability to initiate rotation at specific LWSs [119]. For example, the straight-bladed VAWT often lacks self-starting capability under these conditions primarily due to its aerodynamic design, which can cause flow separation and insufficient lift generation. At low $V_\infty$, the rotor may fail to produce enough aerodynamic forces to overcome static friction and inertia, resulting in an inability to rotate [120].

In contrast, the aerodynamic design of embossed-bladed VAWTs enhances the self-starting capabilities. The embossed design modifies the flow around the blade, creating vortices that facilitate lift and reduce drag. This modification allows for improved performance at lower speeds, as the airflow interacts more favorably with the blade surfaces, generating the necessary torque to initiate rotation. Based on recommendations by Dominy et al. [48], our study employed a three-bladed rotor to enhance self-starting capabilities compared to a two-bladed configuration. This design choice aligns with aerodynamic principles, as having more blades can facilitate smoother airflow interaction, thereby enhancing lift and reducing the risk of stall at lower speeds.

In our evaluation, we examined four distinct scenarios to assess the performance of VAWTs, as detailed in Table 3. The first two scenarios used the NACA0015 airfoil for both straight-bladed and embossed-bladed VAWTs, while the last two scenarios employed the NACA0015-Mod airfoil for the same blade configurations. At $V_\infty$ of 1 m $s^{-1}$ and 1.5 m $s^{-1}$, neither type of VAWT demonstrated the ability to initiate self-starting rotation. These findings highlight the limitations of both airfoil designs under LWS conditions, emphasizing the importance of aerodynamic efficiency in achieving self-starting capabilities.

The inability of both airfoil designs to self-start at LWS conditions is due to insufficient lift generation and excessive drag. Specifically, at 1 m $s^{-1}$ and 1.5 m $s^{-1}$, the flow dynamics around the blades fail to provide sufficient force to overcome the rotor's inertia, preventing the initiation of rotation. However, the NACA0015-Mod airfoil used in the embossed-bladed VAWT showed promise, as it was able to begin rotation at a $V_\infty$ of 2 m $s^{-1}$, reaching a rotational speed of 1 rpm (refer to Fig. 11). This outcome suggests that the aerodynamic improvements offered by the NACA0015-Mod airfoil can significantly enhance the operational threshold for self-starting. The design modifications improve the L/D, making it easier for the rotor to overcome inertia and static friction at lower $V_\infty$ [121].

The performance of embossed-bladed VAWTs utilizing the NACA0015-Mod and NACA0015 airfoils demonstrated effective self-starting capabilities when the $V_\infty$ reached 2.5 m $s^{-1}$. This ability results from the enhanced aerodynamic properties of the embossed blades, which improve lift generation and reduce drag, enabling the rotor to more effectively overcome inertia at lower $V_\infty$. In contrast, straight-bladed VAWTs using the same airfoils were unable to self-start at this $V_\infty$. The inability of the straight-bladed design to initiate rotation is due to its less favorable aerodynamic characteristics at low $V_\infty$. The straight blades often experience flow separation, leading to a significant reduction in lift and increased drag. As a result, these VAWTs cannot generate sufficient torque to initiate rotation, highlighting the importance of blade design in optimizing performance.

At a $V_\infty$ of 2.5 m $s^{-1}$, the embossed-bladed VAWT with the NACA0015-Mod airfoil achieved a rotational speed of 3 rpm. This indicates that modifications to the NACA0015-Mod airfoil enhanced aerodynamic efficiency, resulting in better flow management around the blades. Conversely, the same VAWT equipped with the NACA0015 airfoil only managed to achieve a rotational speed of 2 rpm, as shown in Table 4. This difference in performance highlights the critical role of airfoil design in enhancing the operational capabilities of VAWTs, particularly in their ability to self-start and operate efficiently at varying $V_\infty$.

The evaluation of VAWTs with embossed blades revealed a distinct advantage in rotational performance with increasing $V_\infty$. Specifically, the embossed-bladed VAWTs showed significant improvements in rotation rates, achieving 5 rpm for the NACA 0015-Mod airfoil and 4 rpm for the NACA 0015 airfoil at 3 m $s^{-1}$. In contrast, straight-bladed VAWTs exhibited limited performance, maintaining the same low rotation rates at 3 m $s^{-1}$ as at 2.5 m $s^{-1}$. This stagnation highlights the inherent aerodynamic inefficiencies of the straight-bladed design, which struggles to harness kinetic energy from the airflow due to flow

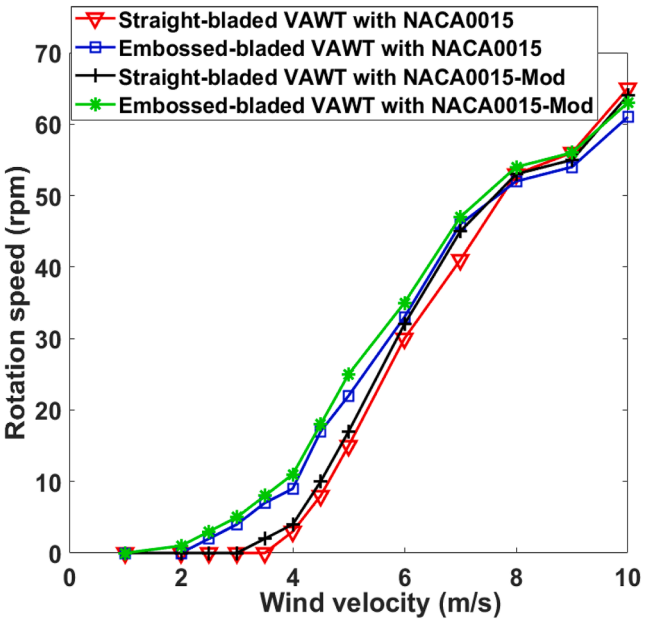


**Fig. 11.** Comparison of rotation speed at different wind speeds (rpm).

**Table 4**
Comparison of rotation speeds (rpm) at different wind velocities.

| Wind velocity ($m\ s^{-1}$) | Straight-bladed with NACA0015 | Embossed-bladed with NACA0015 | Straight-bladed with NACA0015-Mod | Embossed-bladed with NACA0015-Mod |
|---|---|---|---|---|
| 1 | 0 | 0 | 0 | 0 |
| 2 | 0 | 0 | 0 | 1 |
| 2.5 | 0 | 2 | 0 | 3 |
| 3 | 0 | 4 | 0 | 5 |
| 3.5 | 0 | 7 | 2 | 8 |
| 4 | 3 | 9 | 4 | 11 |
| 4.5 | 8 | 17 | 10 | 18 |
| 5 | 15 | 22 | 17 | 25 |
| 6 | 30 | 33 | 32 | 35 |
| 7 | 41 | 46 | 45 | 47 |
| 8 | 53 | 52 | 53 | 54 |
| 9 | 56 | 54 | 55 | 56 |
| 10 | 65 | 61 | 64 | 63 |

separation and increased drag at lower $V_\infty$.

As the $V_\infty$ increased to 3.5 m $s^{-1}$, the NACA0015-Mod airfoil for straight-bladed VAWTs achieved a rotation speed of 2 rpm. However, the NACA0015 airfoil in the straight-bladed configuration failed to demonstrate self-starting capability, highlighting its significant limitations in effectively harnessing wind energy. Conversely, the embossed-bladed VAWTs excelled, reaching rotational speeds of 8 rpm for the NACA0015-Mod and 7 rpm for the NACA0015 airfoils. This performance illustrates the superior aerodynamic characteristics of the embossed design, which not only enhances lift generation but also minimizes stall risk, facilitating efficient energy capture at varying $V_\infty$.

In comparison, findings from a separate study on a conventional Darrieus VAWT with symmetric airfoils highlighted its inability to produce meaningful output power until reaching a $V_\infty$ of 3.65 m $s^{-1}$. This underscores the critical limitations of traditional VAWT designs in capturing kinetic energy for electrical power generation at lower $V_\infty$. In stark contrast, the hybrid Darrieus-Savonius VAWT evaluated in the same study demonstrated self-starting capabilities at a lower $V_\infty$ of 2.81 m $s^{-1}$, demonstrating improved performance compared to conventional designs [53]. However, our findings indicate that embossed-bladed VAWTs outperform both the traditional Darrieus and hybrid Darrieus-Savonius VAWTs, demonstrating effective self-starting and higher rotational speeds at lower wind conditions. This performance advantage can be attributed to the enhanced aerodynamic features of the embossed blades, which optimize flow dynamics and energy conversion efficiency.

At a $V_\infty$ of 4 m $s^{-1}$, the NACA0015 airfoil used in the straight-bladed VAWT achieved a rotational speed of 3 rpm. However, the embossed-bladed VAWTs significantly outperformed this configuration, with the NACA0015-Mod airfoil reaching an impressive maximum of 11 rpm and the NACA0015 airfoil reaching 9 rpm. This stark contrast highlights the embossed-bladed design's superior aerodynamic efficiency, which allows for more effective lift generation and reduced drag, facilitating enhanced energy capture.

In this context, the straight-bladed VAWT with the NACA0015 airfoil exhibited the lowest rotation speed among all tested VAWTs, highlighting its limitations in self-starting and overall performance. Conversely, the embossed-bladed VAWT with the NACA0015-Mod airfoil not only demonstrated superior self-starting capabilities but also achieved the highest rotation rates in the study. This advantage can be attributed to the optimized flow dynamics around the embossed blades, which help maintain laminar flow and minimize stall risk, thus enhancing overall efficiency at various $V_\infty$.

A triangular dimple rotor was evaluated, demonstrating a significant peak performance improvement of approximately 13.6 % compared to a dimple-free Darrieus VAWT at a $V_\infty$ of 4 m $s^{-1}$ [122]. While this result indicates improvements in other rotor designs, it is essential to note that the embossed-bladed VAWTs in our study consistently exhibited superior performance metrics, including higher rotation speeds and better self-starting capabilities at lower $V_\infty$. This suggests that the embossed blade design offers a more reliable and efficient solution for harnessing wind energy compared to both traditional designs and other alternative rotor configurations.

This trend of enhanced performance continued as $V_\infty$ increased, as illustrated in Table 4. At a $V_\infty$ of 4.5 m $s^{-1}$, the embossed-bladed VAWTs utilizing the NACA0015-Mod airfoil achieved a peak rotational speed of 18 rpm. In stark contrast, the straight-bladed VAWTs using the NACA0015 airfoil exhibited the lowest rotational speed of 8 rpm. Additionally, the straight-bladed VAWTs with the NACA0015-Mod airfoil recorded a rotational speed of 10 rpm, while the embossed-bladed VAWTs using the NACA0015 airfoil achieved a rotational speed of 17 rpm. This data further reinforces the superior aerodynamic efficiency of the embossed-bladed design, which effectively captures wind energy and translates it into higher rotational speeds.

The marked performance differences among the various configurations highlight the crucial role of airfoil design in optimizing VAWT performance. The embossed blades' ability to maintain laminar flow and reduce drag contributes significantly to their higher rotational speeds, even under varying wind conditions. Conversely, the straight-bladed designs, particularly with the NACA0015 airfoil, struggle to match performance levels, underscoring their limitations in effectively capturing kinetic energy.

In a related study on VAWT designs, Su et al. [123] explored a novel straight-bladed VAWT featuring three pairs of blades, each consisting of a fixed main blade and a rotatable auxiliary blade. Their findings indicated that this innovative design outperformed a traditional three-blade H-type rotor in terms of $C_p$ at $V_\infty$ ranging from 4.54 m $s^{-1}$ to 8.82 m $s^{-1}$. While this new design represents an advancement in straight-bladed VAWTs, it is essential to note that the embossed-bladed VAWTs in our study consistently demonstrated superior rotational speeds and overall performance metrics, particularly at lower $V_\infty$. This suggests that the embossed blade design remains a more effective solution for harnessing wind energy in diverse conditions, thereby reinforcing its viability for VAWT applications.

At a $V_\infty$ of 5 m $s^{-1}$, the embossed-bladed VAWTs utilizing the NACA0015-Mod airfoil achieved the highest rotational speed of 25 rpm. In contrast, the NACA 0015 airfoil in straight-bladed VAWTs recorded the lowest rotational speed of 15 rpm. Additionally, the NACA 0015 airfoil for embossed-bladed VAWTs reached a rotational speed of 22 rpm, while the NACA 0015-Mod airfoil in straight-bladed VAWTs achieved a speed of 17 rpm. This trend underscores the superior aerodynamic efficiency and self-starting capabilities of the embossed-bladed designs, which are better equipped to harness wind energy effectively at increasing $V_\infty$.

The significant performance gap between various rotor configurations highlights the impact of airfoil design on the efficiency and operational capabilities of VAWTs. The NACA0015-Mod airfoil's ability to achieve higher rotational speeds reflects its optimized shape, which enhances lift and reduces drag, thereby facilitating superior energy conversion at a $V_\infty$ of 5 m $s^{-1}$. Conversely, straight-bladed configurations struggle to match these performance levels, emphasizing their limitations in effectively capturing kinetic energy.

In a related study, Kavade et al. [124] explored a vertical axis wind turbine (VAWT) design based on the NACA 0021 airfoil, featuring a C = 9.50 cm, a $H = 60$ cm, and a $D = 60$ cm. Their experimental measurements, conducted at $V_\infty$ ranging from 1 to 12 m $s^{-1}$, revealed that the fixed-pitch turbine could not initiate rotation at lower $V_\infty$, specifically between 1 and 5 m $s^{-1}$, due to inadequate and even negative torque. This finding underscores the challenges faced by certain VAWT designs in effectively harnessing wind energy at lower operational thresholds.

Additionally, Xu et al. [125] conducted laboratory experiments to evaluate the self-starting capabilities of VAWTs utilizing NACA0018, NACA2418, and NACA4418 airfoils at β of 0°, 5°, and 10° Their

experimental setup featured blades with a C of 13.33 cm, three blades per rotor, a H of 40 cm, a D of 50 cm, and a σ of 0.80. Their results indicated that at a $V_\infty$ of 5 m $s^{-1}$, the VAWT with the NACA2418 airfoil exhibited a 20 % decrease in self-starting time at a β of 10° and a 12 % reduction at 5° compared to a β of 0° While these studies demonstrate advancements in VAWT designs, it is essential to note that the embossed-bladed VAWTs in our investigation consistently outperformed traditional configurations. The enhanced rotational speeds and effective self-starting capabilities of the embossed-bladed designs reaffirm their superiority in harnessing wind energy efficiently, especially at varying wind conditions.

The NACA0015-Mod airfoil employed in embossed-bladed VAWTs consistently demonstrated superior self-starting capabilities compared to other VAWT configurations. At a $V_\infty$ of 6 m $s^{-1}$, it achieved an impressive rotational speed of 35 rpm, outpacing the NACA0015 airfoil for the same type of VAWT, which recorded a lower $V_\infty$. In contrast, the straight-bladed VAWTs utilizing the NACA0015-Mod and NACA0015 airfoils reached rotational speeds of 32 rpm and 30 rpm, respectively, at the same $V_\infty$. Interestingly, the rotational speeds for these configurations exhibited much smaller variation at this $V_\infty$, indicating a more consistent performance among straight-bladed designs, albeit at lower overall $V_\infty$. The findings highlight the improved aerodynamic efficiency of the NACA 0015-Mod airfoil, which not only enables faster self-starting but also optimizes lift generation, leading to higher rotational speeds. The ability of the embossed-bladed VAWT to maintain elevated performance levels at varying wind conditions reinforces its advantages over traditional designs.

In a related study by Mazarbhuiya et al. [126], a 20 cm blade attachment was added to a NACA63–415 blade of a VAWT operating at a β of +5° Their results indicated that VAWT configurations featuring attachments on both sides of the blade's upper position achieved a maximum $C_p$ of 0.13 at a TSR of 1.8 and a $V_\infty$ of 6.0 m $s^{-1}$. This performance surpassed all other configurations tested and represented a 4.34 % increase in $C_p$ compared to the same blade without attachments. Such enhancements highlight the potential for optimizing VAWT designs through innovative modifications to blade profiles.

Moreover, it was observed that under turbulent conditions, significant improvements in power performance occurred as $V_\infty$ increased from 5 m $s^{-1}$ to 10 m $s^{-1}$, with only slight additional gains noted at higher $V_\infty$ [127]. This finding emphasizes the importance of optimizing VAWT configurations to harness wind energy effectively, particularly in varying and turbulent wind environments. The superior performance of the embossed-bladed VAWTs, especially at lower $V_\infty$, positions them as a reliable and efficient option for wind energy capture, reinforcing their viability for practical applications.

At the $V_\infty$ of 7 m $s^{-1}$, the embossed-bladed VAWT utilizing the NACA0015-Mod airfoil achieved an impressive rotational speed of 47 rpm, marking it the fastest option among the four configurations evaluated. This demonstrates the superior self-starting capability and aerodynamic efficiency of the NACA0015-Mod airfoil, which continues to excel at higher $V_\infty$. Moreover, a Darrieus VAWT with a σ of 0.417 or higher has been shown to self-start in less than 30 s at a $V_\infty$ of 7.9 m $s^{-1}$ [128]. This rapid self-starting capability is crucial for maximizing energy capture in fluctuating wind conditions, highlighting the design advantages that enhance operational effectiveness.

As the $V_\infty$ increased to 8 m $s^{-1}$, the NACA0015-Mod airfoil for embossed-bladed VAWTs achieved the highest rotational speed of 54 rpm among all configurations tested. Notably, the NACA0015 airfoil for straight-bladed VAWTs and the NACA0015-Mod airfoil for straight-bladed VAWTs reached similar performance levels, reaching 53 rpm. In contrast, the NACA0015 airfoil for embossed-bladed VAWTs recorded the lowest rotational speed at 52 rpm. Although these rotation values were closely aligned, they reiterate the trend observed throughout the study, where the NACA0015 airfoil for embossed-bladed VAWTs consistently exhibited lower rotational speeds than its NACA0015-Mod counterpart. The findings highlight the continued dominance of the NACA0015-Mod airfoil in embossed-bladed VAWTs, showcasing its superior performance in harnessing wind energy efficiently. The slight variations in rotation speeds among the other configurations at this $V_\infty$ further emphasize the reliability of the embossed-bladed design, reinforcing its position as a top choice for effective wind energy conversion.

At a $V_\infty$ of 9 m $s^{-1}$, both the NACA0015-Mod airfoil for embossed-bladed VAWTs and the NACA0015 airfoil for straight-bladed VAWTs achieved the highest rotational speed of 56 rpm. Following closely, the NACA0015-Mod airfoil for straight-bladed VAWTs and the NACA0015 airfoil for embossed-bladed VAWTs reached rotational speeds of 55 rpm and 54 rpm, respectively. This performance illustrates the competitive edge of the NACA0015 airfoil designs across both configurations at this $V_\infty$.

As the $V_\infty$ increased to 10 m $s^{-1}$, the NACA0015 airfoil for straight-bladed VAWTs recorded the highest rotation speed of 65 rpm. In contrast, the NACA0015 airfoil for embossed-bladed VAWTs exhibited the lowest rotation speed at this level, achieving 61 rpm. Meanwhile, the NACA0015-Mod airfoil for straight-bladed VAWTs and the NACA0015-Mod airfoil for embossed-bladed VAWTs maintained impressive performances with rotational speeds of 64 rpm and 63 rpm, respectively.

Overall, the NACA0015-Mod airfoil for embossed-bladed VAWTs demonstrated superior self-starting capabilities and rotational speeds across the range of $V_\infty$ from 2 to 9 m $s^{-1}$. Notably, the NACA0015 airfoil for embossed-bladed VAWTs outperformed the NACA0015 airfoil for straight-bladed VAWTs regarding self-starting ability and rotational speed up to a $V_\infty$ of 8 m $s^{-1}$.

The aerodynamic advantages of embossed-bladed VAWTs can be attributed to their ability to inhibit the separation zone and weaken vortices, allowing them to dissipate more rapidly. The design of the embossed blades enhances flow attachment, resulting in reduced vorticity sizes and a smaller wake region downstream of the rotor. This contrasts with straight-bladed VAWTs, which tend to experience larger vortices on their surfaces [129]. By stabilizing the flow and mitigating vortex impacts, the embossed blade design decreases vibrations and fatigue stresses on the rotor shaft, ultimately enhancing the rotor velocity of the VAWT.

Fig. 12 and Table 5 illustrate the rotational speeds of the tested VAWTs in radians per second (rad $s^{-1}$), highlighting the distinct performance characteristics of each design in response to varying wind conditions.

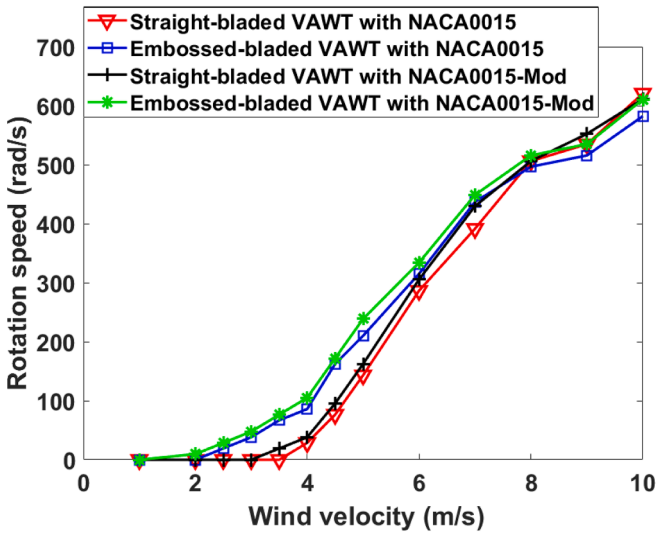


**Fig. 12.** Comparison of rotation speed at wind velocities of 1 to 10 m $s^{-1}$.

**Table 5**
Comparison of rotation speed at wind velocities of 1 to 10 m $s^{-1}$.

| (m $s^{-1}$) | Straight-bladed with NACA0015 | Embossed-bladed with NACA0015 | Straight-bladed with NACA0015-Mod | Embossed-bladed with NACA0015-Mod |
|---|---|---|---|---|
| 1 | 0 | 0 | 0 | 0 |
| 2 | 0 | 0 | 0 | 9.55 |
| 2.5 | 0 | 19.10 | 0 | 28.65 |
| 3 | 0 | 38.20 | 0 | 47.75 |
| 3.5 | 0 | 66.85 | 19.10 | 76.40 |
| 4 | 28.65 | 85.95 | 38.20 | 105.05 |
| 4.5 | 76.48 | 162.35 | 95.50 | 171.90 |
| 5 | 143.25 | 210.10 | 162.35 | 238.75 |
| 6 | 286.5 | 315.15 | 305.60 | 334.25 |
| 7 | 391.55 | 437 | 429.75 | 448.75 |
| 8 | 506.15 | 496.6 | 506.15 | 515.70 |
| 9 | 534.8 | 515.7 | 552.25 | 534.80 |
| 10 | 620.75 | 582.25 | 611.20 | 601.65 |

### *5.4. Experimental study of the self-starting force required for the Darrieus VAWT*

To initiate the rotation of a VAWT at different $V_\infty$, the force required to overcome inertia and initiate motion must be generated. This requirement can lead to increased energy consumption during startup, which detracts from actual electricity generation. Fig. 13 and Table 6 compare the forces needed for self-starting the NACA0015 and NACA0015-Mod airfoils across both straight-bladed and embossed-bladed VAWTs at varying $V_\infty$.

Darrieus VAWTs exhibit limited self-starting capabilities at LWS, which necessitates a higher self-starting force at these speeds compared to moderate and high $V_\infty$. At zero m $s^{-1}$, there is no wind, resulting in a startup force of zero for all WT configurations. As $V_\infty$ increases to 1 m $s^{-1}$, Darrieus VAWTs with embossed blades demonstrate a lower self-starting force requirement than their straight-bladed counterparts. Notably, the embossed modified NACA0015 airfoil required the lowest self-starting force of just 0.83 N at 1 m $s^{-1}$, underscoring its superior efficiency. The modified shape of the NACA0015 airfoil in straight-bladed VAWTs also required less startup force than the unmodified NACA0015 airfoil. This improvement can be attributed to the enhanced lift characteristics and reduced drag of the modified airfoil design, effectively lowering the force needed for self-starting.

Furthermore, Yang et al. [130] discovered that while increases in turbulence intensity have a minor effect on the self-starting performance of VAWTs, they significantly improve wind energy utilization within a specific turbulence range, leading to an average power gain of 1.41 %.

At a $V_\infty$ of 2 m $s^{-1}$, the Darrieus VAWTs demonstrated a notable decrease in the self-starting force required compared to the 1 m $s^{-1}$ condition. This improvement highlights the significant influence of aerodynamic design on turbine performance. Investigations at this $V_\infty$ revealed that combining embossed blades with modified NACA0015 airfoils resulted in a lower self-starting force requirement for this VAWT configuration than for the other three Darrieus VAWTs tested. Reducing the self-starting force is critical, as it indicates a more efficient conversion of wind energy into rotational energy. Specifically, using embossed blades instead of straight blades reduced the required self-starting force from 0.80 N to 0.72 N. This enhancement can be attributed to the improved flow characteristics around the embossed blades, which facilitate smoother and more stable airflow, thereby reducing drag and allowing for quicker initiation of rotation. Moreover, modifying the NACA0015 airfoil shape further optimized the performance of straight-bladed Darrieus VAWTs. The self-starting force for unmodified straight-bladed VAWTs was recorded at 0.80 N, while the modified version required only 0.77 N. This reduction underscores the role of airfoil design in minimizing resistance and improving lift characteristics, collectively enhancing the turbine's ability to self-start under low wind conditions.

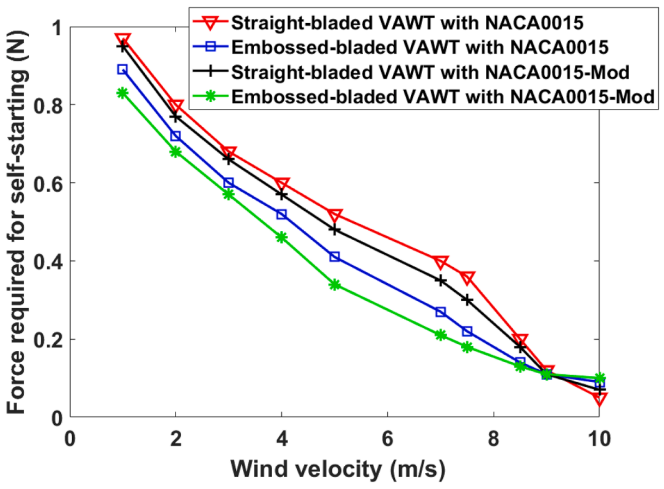


**Fig. 13.** Comparison of required force self-starting at different wind speeds.

**Table 6**
Comparison of required force self-starting at different wind speeds.

| Wind Speed (m $s^{-1}$) | Straight-bladed with NACA0015 (N) | Embossed-bladed with NACA0015 (N) | Straight-bladed with NACA0015-Mod (N) | Embossed-bladed with NACA0015-Mod (N) |
|---|---|---|---|---|
| 0 | 0 | 0 | 0 | 0 |
| 1 | 0.97 | 0.89 | 0.95 | 0.83 |
| 2 | 0.80 | 0.72 | 0.77 | 0.68 |
| 3 | 0.68 | 0.60 | 0.66 | 0.57 |
| 4 | 0.60 | 0.52 | 0.57 | 0.46 |
| 5 | 0.52 | 0.41 | 0.48 | 0.34 |
| 7 | 0.40 | 0.27 | 0.35 | 0.21 |
| 7.50 | 0.36 | 0.22 | 0.30 | 0.18 |
| 8.5 | 0.20 | 0.14 | 0.18 | 0.13 |
| 9 | 0.12 | 0.11 | 0.11 | 0.11 |
| 10 | 0.05 | 0.09 | 0.07 | 0.10 |

At a $V_\infty$ of 3 m $s^{-1}$, the Darrieus VAWTs demonstrated a significant reduction in the required self-starting force compared to the lower $V_\infty$ of 2 and 1 m $s^{-1}$. This trend highlights the positive effect of increasing $V_\infty$ on turbine performance, as higher $V_\infty$ enhances the lift generated by the blades, making it easier to initiate rotation. Among the configurations tested, the embossed blades equipped with the modified NACA0015 airfoil exhibited the lowest self-starting force, highlighting the aerodynamic advantages provided by this design. Conversely, the straight-blade VAWT with the original NACA0015 airfoil consistently required the highest self-starting force at this $V_\infty$. This observation indicates that the traditional design struggles to overcome initial resistance due to less efficient airflow characteristics. Straight blades are more prone to flow separation, leading to increased drag and a higher torque requirement to initiate movement.

In a comparative analysis, a standard Darrieus VAWT configuration derived using the one-factor-at-a-time method was evaluated across varying $V_\infty$. The findings revealed that the standard Darrieus configuration was unable to generate power at $V_\infty$ below 3.85 m $s^{-1}$, indicating its limited capability under lower wind conditions. In contrast, the optimized Darrieus VAWT showcased superior performance, demonstrating the ability to self-start at a $V_\infty$ as low as 3.22 m $s^{-1}$. This enhanced self-starting capability can be attributed to the aerodynamic refinements incorporated into the design, allowing for better energy conversion and utilization of the kinetic energy in the airflow [131].

At a $V_\infty$ of 4 m $s^{-1}$, the embossed-bladed VAWT using the NACA0015-Mod airfoil demonstrated the lowest self-starting force requirement at 0.46 N. This finding highlights the effectiveness of the modified airfoil design in enhancing the turbine's aerodynamic performance and efficiency, allowing it to better harness the kinetic energy of the wind. In

contrast, the straight-bladed VAWT equipped with the original NACA0015 airfoil required the highest self-starting force of 0.60 N among the four configurations tested. This indicates that the straight-bladed design suffers from greater aerodynamic drag and flow separation, necessitating a higher torque to initiate rotation.

Additionally, a study conducted by Khalid et al. [132] investigated the advantages of dual-stage VAWTs across varying $V_\infty$. Their findings revealed that at a $V_\infty$ of 4 m $s^{-1}$, implementing phase angles of 30° and 90° significantly reduced the starting time compared to a single-stage VAWT. This improvement can be attributed to the enhanced aerodynamic interaction between the blades in the dual-stage configuration, allowing for better lift generation and minimizing the impact of turbulent wake regions on self-starting performance. Overall, the results at a $V_\infty$ of 4 m $s^{-1}$ underscore the critical role of aerodynamic design in optimizing self-starting capabilities and performance in Darrieus VAWTs.

At a $V_\infty$ of 5 m $s^{-1}$, the embossed-bladed VAWT utilizing the NACA0015-Mod airfoil demonstrated the lowest self-starting force requirement of 0.34 N. This represents a significant reduction of approximately 34.6 % compared to the straight-bladed VAWT equipped with the original NACA0015 airfoil, which required a self-starting force of 0.52 N. This disparity highlights the adverse effects of increased drag and flow separation associated with the straight-bladed design.

At a $V_\infty$ of 7 m $s^{-1}$, the straight-bladed Darrieus VAWT equipped with the NACA0015 airfoil exhibited the highest self-starting force requirement of 0.40 N. By employing the modified NACA 0015 airfoil, this force requirement was reduced to 0.35 N, reflecting a 12.5 % decrease. More significantly, the transition from straight blades to embossed blades resulted in a substantial reduction of the startup force from 0.40 N to 0.27 N, indicating a remarkable 32.5 % improvement in startup performance. This shows that the embossed blades have a more pronounced effect on the self-starting capabilities at a $V_\infty$ of 7 m $s^{-1}$ compared to the modifications made to the NACA0015 airfoil.

Furthermore, the combined use of embossed blades with the modified NACA0015 airfoil led to an even more impressive reduction in the required startup force from 0.40 N to 0.21 N, showcasing a 47.5 % enhancement in startup performance. In another study, the 3-PB VAWT design, consisting of three blades divided into three segments of equal height (H/3), was evaluated. The aerodynamic performance of their design, with helix angles ranging from 60° to 120°, was thoroughly analyzed using three-dimensional numerical simulations at a $V_\infty$ of 7 m $s^{-1}$. Their results showed a significant reduction in the variation of the VAWT's torque coefficient from its average value, achieving a 40 % decrease at a low TSR of 0.44 compared to a baseline 3-PB VAWT with a 60° helix angle [133].

At a $V_\infty$ of 7.5 and 8.5 m $s^{-1}$, the trend observed at lower $V_\infty$ values continued, with each of the four Darrieus VAWTs requiring less startup force. Specifically, the combined use of the modified NACA0015 airfoil and embossed blades resulted in the lowest startup force requirements across the tested $V_\infty$ range from 1 to 9 m $s^{-1}$. Integrating embossed blades with modified airfoil shapes, such as the NACA0015, significantly enhances the aerodynamic performance of the VAWTs. The modified NACA0015 airfoil shape not only improves lift characteristics but also reduces drag, thereby complementing the benefits provided by the embossed blades. This synergy between the modified airfoil and embossed blades illustrates their crucial role in enhancing the overall performance of Darrieus VAWTs, particularly in reducing startup force requirements. The reduction in startup force not only enhances energy conversion efficiency but also improves the self-starting capabilities of VAWTs under various wind conditions.

At a $V_\infty$ of 9 m $s^{-1}$, as expected, each of the Darrieus VAWTs required a lower startup force compared to the previously examined $V_\infty$. The transition from straight blades to embossed blades resulted in a slight reduction in startup force for the VAWT, decreasing from 0.12 N to 0.11 N. This reduction is considerably smaller than the decreases observed at lower $V_\infty$, indicating diminishing returns as $V_\infty$ increases. Additionally, at the same $V_\infty$ of 9 m $s^{-1}$, using the modified NACA0015 airfoil led to a reduced startup force requirement for the straight-bladed Darrieus VAWT, also decreasing from 0.12 N to 0.11 N. However, for the turbine with embossed blades, changing the airfoil shape did not yield any significant improvement in self-starting, as the required startup force remained at 0.11 N. Results from Sun et al. [134] indicated that the VAWT with a β of −4° exhibited a shorter self-starting time at the higher $V_\infty$ of 9 m $s^{-1}$, highlighting the importance of optimizing both blade design and operational parameters for enhanced performance.

At a $V_\infty$ of 10 m $s^{-1}$, an unexpected trend was observed: the combined use of embossed blades and a modified NACA0015 airfoil led to an increase in startup force from 0.05 N to 0.10 N. This observation contradicts the performance characteristics noted at lower $V_\infty$, where such configurations typically reduce startup force. Modifying the NACA0015 airfoil also resulted in a higher startup force requirement for VAWTs equipped with embossed blades, a phenomenon not observed at lower speeds.

In summary, embossed-bladed VAWTs consistently require a lower self-starting force than straight-bladed VAWTs across $V_\infty$ values from 1 to 9 m $s^{-1}$. This advantage stems from the enhanced ability of embossed blades to overcome static friction, effectively reducing the torque needed to initiate rotation. Their aerodynamic design allows for better management of resisting torque, enabling embossed-bladed VAWTs to self-start at lower wind speeds. In contrast, straight-bladed VAWTs often lack this capability under similar conditions [129].

## 6. Conclusions

This research investigated the use of an embossed-bladed VAWT to enhance the self-starting capabilities of the Darrieus H-rotor compared to the commonly used straight solid blade. A total of forty-four rotors were selected and tested at a Re of 40,673. The study yielded the following results:

- The study demonstrated that the NACA0015-Mod rotor outperformed the original NACA0015 rotor, achieving a maximum $C_p$ of 0.171, at a Re of 40,673. This represents approximately a 12.50 percent improvement over the unmodified version. This enhancement underscores the significant impact of design modifications on the aerodynamic efficiency of VAWTs, particularly at lower TSRs.
- In comparison, research on bionic airfoils indicated increases in the $C_p$, ranging from 3.42 % to 7.35 % at specific TSRs. While these enhancements are practical, they do not match the greater and more consistent improvements offered by the NACA0015-Mod rotor across a broader operational range.
- Studies focusing on low Re airfoils, such as NACA0021, revealed a maximum $C_p$ of approximately 0.3263 at higher TSRs. Although this value is higher than that of the NACA0015 rotor, the significant improvements of the NACA0015-Mod rotor at lower TSRs suggest it is better suited for scenarios requiring efficiency across varying wind conditions, making it more adaptable for small-scale applications.
- Other investigations into VAWT designs, such as J-shaped, straight-bladed configurations, demonstrated improvements of approximately 12.35 % in power generation at elevated TSRs. While this enhancement is significant, the consistent performance of the NACA0015-Mod rotor across different TSRs highlights its broader applicability. Additional modifications, including negatively cambered airfoils and the addition of circular dimples on blade surfaces, yielded increases in $C_p$ of 8.8 % and 5.18 %, respectively. Although these results are beneficial, they fall short of the 12.50 % gain achieved by the NACA0015-Mod rotor.
- Other design strategies, such as using porous deflectors, leading-edge serrations, and vented airfoil configurations, reported enhancements in $C_p$ ranging from 7 % to 20 %. While these alternative approaches offer potential improvements, the NACA0015-Mod rotor continues to excel, primarily due to its ability to maintain performance benefits

at both low and high TSRs, which is crucial for practical VAWT applications.

- The consistent efficiency gains of the NACA0015-Mod rotor, particularly in the lower TSR range, give it an advantage over alternative rotor designs like blades with slit gust filters or semi-flexible trailing edges, which tend to exhibit localized improvements. Despite the adaptability of configurations such as hybrid rotors and variable swept area designs, the simple modifications of the NACA0015-Mod rotor offer a more practical approach to enhancing VAWT performance.
- Overall, the enhanced aerodynamic profile of the NACA0015-Mod rotor leads to more efficient energy conversion, which provides significant performance benefits over other modifications. This study suggests that relatively simple design adjustments, such as airfoil modifications and optimized blade geometries, can yield substantial improvements in performance, making them a practical choice for advancing the efficiency of small-scale VAWTs in varying wind conditions.
- This study investigated the performance of the NACA0015-Mod airfoil for embossed-bladed VAWTs, demonstrating that it can achieve self-starting capability at a minimum $V_\infty$ of 2 m $s^{-1}$. Additionally, for embossed-bladed VAWTs, the minimum self-starting $V_\infty$ was reduced from 4 m $s^{-1}$ to 2.5 m $s^{-1}$ with the NACA0015 airfoil. Other studies have shown that conventional Darrieus VAWTs with symmetric airfoils face significant limitations at LWS, as they cannot produce meaningful output power until reaching a $V_\infty$ of 3.65 m $s^{-1}$.
- Additionally, designs that integrate features from both Darrieus and Savonius VAWTs demonstrate improved self-starting capabilities, achieving rotation at a lower $V_\infty$ of 2.81 m $s^{-1}$. This comparison highlights the advantages of hybrid and modified airfoil approaches, such as the NACA0015-Mod airfoil on embossed blades, in overcoming the challenges of self-starting and low-speed performance.
- At a $V_\infty$ of 4 m $s^{-1}$, the straight-bladed VAWT utilizing the NACA0015 airfoil achieved a rotational speed of 3 rpm. In stark contrast, the embossed-bladed VAWTs demonstrated significantly superior performance, with the NACA0015-Mod airfoil reaching an impressive maximum rotational speed of 11 rpm, representing an increase of approximately 267 % compared to the straight-bladed configuration. The NACA0015 airfoil for embossed-bladed VAWTs also performed admirably, achieving a rotational speed of 9 rpm, corresponding to a 200 % increase over the straight-bladed design. Additionally, other studies showed that a triangular dimple rotor achieved a peak performance improvement of approximately 13.6 % compared to a dimple-free Darrieus VAWT at the same $V_\infty$ of 4 m $s^{-1}$.
- The embossed blade design not only provides significant improvements in energy capture but also serves as a more reliable and efficient solution for harnessing wind energy compared to traditional designs and other alternative rotor configurations.
- A novel straight-bladed VAWT demonstrated significant improvements in the $C_p$ compared to a traditional three-blade H-type rotor, particularly within the $V_\infty$ range of 4.54 m $s^{-1}$ to 8.82 m $s^{-1}$. However, it is important to emphasize that the embossed-bladed VAWTs examined in our study consistently outperformed both the novel straight-bladed design and the H-type rotor, with superior performance especially evident at lower $V_\infty$.
- The NACA0015-Mod airfoil used in the embossed-bladed VAWTs achieved the highest rotational speeds across the operational range of 2 to 9 m $s^{-1}$. This indicates that while the new straight-bladed VAWT represents a promising advancement, the embossed-bladed VAWTs provide a more effective solution for harnessing wind energy, showcasing enhanced efficiency and performance even at lower $V_\infty$.
- The NACA0015 airfoil for embossed-bladed VAWTs required the lowest starting force at $V_\infty$ ranging from 1 to 9 m $s^{-1}$, compared to the NACA0015 airfoil for straight-bladed VAWTs. These enhancements are attributed to the embossed design's ability to maintain attached airflow to the blades, effectively suppressing flow separation.
- While existing research acknowledges the challenges fixed-pitch turbines face at LWSs, our work emphasizes the need for design innovations to address these issues effectively. By exploring modifications seen in embossed-bladed VAWTs, we demonstrate that alternative designs can effectively overcome the limitations of fixed-pitch configurations, potentially enabling self-starting capabilities at lower wind velocities.

For future work, research will focus on the embossed-bladed Darrieus VAWT utilized in the present study, investigating the influence of circular, square, and rectangular blades on self-starting capabilities in collaboration with Solar Turbine Arta Energy (Iran) and ABSCUBE Engineering & Education (Australia). Additional airfoils will be studied to enhance the aerodynamic efficiency of the VAWT, along with exploring combinations with Savonius VAWTs. The effect of increasing starting torque using a J-type embossed blade VAWT will also be investigated and compared to the current starting torque.

## Funding

No funding was received

## CRediT authorship contribution statement

**Hossein Seifi Davari:** Writing – original draft, Visualization, Validation, Software, Resources, Project administration, Methodology, Investigation, Funding acquisition, Formal analysis, Data curation, Conceptualization. **Ruxandra Mihaela Botez:** Writing – review & editing, Validation, Supervision, Methodology, Investigation, Data curation, Conceptualization. **Mohsen Seify Davari:** Writing – original draft, Validation, Software, Project administration, Funding acquisition, Data curation, Formal analysis, Visualization. **Harun Chowdhury:** Writing – review & editing. **Hasan Hosseinzadeh:** Validation, Software, Methodology, Formal analysis, Investigation, Project administration, Supervision.

## Declaration of competing interest

The authors have declared no conflict of interest related to this work.

## Data availability

Data will be made available on request.

## References

[1] L.J. Nunes, M. Casau, M.F. Dias, J.C.O. Matias, L.C. Teixeira, Agroforest woody residual biomass-to-energy supply chain analysis: feasible and sustainable renewable resource exploitation for an alternative to fossil fuels, Results in Eng. 17 (2023) 101010, https://doi.org/10.1016/j.rineng.2023.101010.

[2] L.M. Shaker, J.K. Mohammed, A. Basem, R.J. Halbos, R.R. Mahdi, S. A. Mohammed, M.H. Al Lami, Comparative analysis of solar cells and hydrogen fuel: a mini-review, Results in Eng. 23 (2024) 102507, https://doi.org/10.1016/j.rineng.2024.102507.

[3] L.O. Ajuka, R.A. Kazeem, O.A. Kuti, T.C. Jen, A.S. Afolalu, E.T. Akinlabi, Decarbonized automotive fuel: liquefied petroleum gas biosynthesis, benefits and drawbacks, Results in Eng. 101889 (2024), https://doi.org/10.1016/j.rineng.2024.101889.

[4] B. Panbechi, A. Hajinezhad, H. Yousefi, S.F. Moosavian, S. Hajinezhad, Environmental, economic and energy evaluation of alternative fuels for a steam power plant: focus on biodiesel-nanoparticles utilization, Results in Eng. 23 (2024) 102636, https://doi.org/10.1016/j.rineng.2024.102636.

[5] I. Veza, M. Spraggon, I.R. Fattah, M. Idris, Response surface methodology (RSM) for optimizing engine performance and emissions fueled with biofuel: review of RSM for sustainability energy transition, Results in Eng. 18 (2023) 101213, https://doi.org/10.1016/j.rineng.2023.101213.

[6] M. Aravindan, P. Kumar, Hydrogen towards sustainable transition: a review of production, economic, environmental impact and scaling factors, Results in Eng. (2023) 101456, https://doi.org/10.1016/j.rineng.2023.101456.

[7] A.A. Firoozi, M. Tshambane, A.A. Firoozi, S.M. Sheikh, Strategic load management: enhancing eco-efficiency in mining operations through automated technologies, Results in Eng. (2024) 102890, https://doi.org/10.1016/j.rineng.2024.102890.

[8] A. Farooq, W. Alhalabi, Evaluation of hydrogen fuel cell-based systematic vehicular application to promote the green economy using LabVIEW, Results in Eng. 20 (2023) 101607, https://doi.org/10.1016/j.rineng.2023.101607.

[9] M. Umer, N. Abas, S. Rauf, M.S. Saleem, S. Dilshad, GHG Emissions Estimation and Assessment of Pakistan's Power Sector: a Roadmap Towards Low Carbon Future, Results in Eng. 102354 (2024), https://doi.org/10.1016/j.rineng.2024.102354.

[10] A.Y. Ugya, Y. Sheng, H. Chen, Q. Wang, Microalgal bioengineering: a futuristic tool for carbon capture, Results in Eng. (2024) 102990, https://doi.org/10.1016/j.rineng.2024.102990.

[11] J.J. Andreas, C. Burns, J. Touza, A qualitative comparative analysis of the role of the economy in the EU's renewable energy transitions during the 'double crisis, Ecol. Econ. 142 (2017) 81–90, https://doi.org/10.1016/j.ecolecon.2017.06.011.

[12] V.M. Krishna, S.S. Duvvuri, P.V. Sobhan, K. Yadlapati, V. Sandeep, B.K. Narendra, Experimental study on excitation phenomena of renewable energy source driven induction generator for isolated rural community loads, Results in Eng. 21 (2024) 101761, https://doi.org/10.1016/j.rineng.2024.101761.

[13] F.A.A. Ali, Optimizing size and evaluating Techno-Enviro-Economic Feasibility of hybrid renewable energy to power RO/Well unit, Results in Eng. 23 (2024) 102805, https://doi.org/10.1016/j.rineng.2024.102805.

[14] Q. Hassan, S. Algburi, A.Z. Sameen, H.M. Salman, M. Jaszczur, A review of hybrid renewable energy systems: solar and wind-powered solutions: challenges, opportunities, and policy implications, Results in Eng. 101621 (2023), https://doi.org/10.1016/j.rineng.2023.101621.

[15] M.S. Saleem, N. Abas, Optimizing renewable polygeneration: a synergetic approach harnessing solar and wind energy systems, Results in Eng. 21 (2024) 101743, https://doi.org/10.1016/j.rineng.2023.101743.

[16] S. Hasan, A.I. Meem, M.S. Islam, S.S. Proma, S.K. Mitra, Comparative techno-economic analyses and optimization of standalone and grid-tied renewable energy systems for South Asia and Sub-Saharan Africa, Results in Eng.. 21 (2024) 101964, https://doi.org/10.1016/j.rineng.2024.101964.

[17] A. Baz, S.K. Patel, Efficiency-aware machine-learning driven design of solar harvester for renewable energy application, Results in Eng.. (2024) 103050, https://doi.org/10.1016/j.rineng.2024.103050.

[18] A. Al Naimat, D. Liang, Substantial gains of renewable energy adoption and implementation in Maan, Jordan: a critical review, Results in Eng. 101367 (2023), https://doi.org/10.1016/j.rineng.2023.101367.

[19] M. Peyvandi, A. Hajinezhad, S.F. Moosavian, Investigating the intensity of GHG emissions from electricity production in Iran using renewable sources, Results in Eng.. 17 (2023) 100819, https://doi.org/10.1016/j.rineng.2022.100819.

[20] R. Zhang, J. Cao, W. Wang, E. Tan, R. Zhu, W. Chen, Y. Zhang, Research on design strategies and sensing applications of energy storage system based on renewable methanol fuel, Results in Eng. 20 (2023) 101439, https://doi.org/10.1016/j.rineng.2023.101439.

[21] A.A. Imam, A. Abusorrah, M. Marzband, Potentials and opportunities of solar PV and wind energy sources in Saudi Arabia: land suitability, techno-socio-economic feasibility, and future variability, Results in Eng. 21 (2024) 101785, https://doi.org/10.1016/j.rineng.2024.101785.

[22] A.A. Youssef, S. Barakat, E. Tag-Eldin, M.M. Samy, Islanded green energy system optimal analysis using PV, wind, biomass, and battery resources with various economic criteria, Results in Eng. 19 (2023) 101321, https://doi.org/10.1016/j.rineng.2023.101321.

[23] A. Ali, S. Ali, H. Shaukat, E. Khalid, L. Behram, H. Rani, M. Noori, Advancements in piezoelectric wind energy harvesting: a review, Results in Eng.. (2024) 101777, https://doi.org/10.1016/j.rineng.2024.101777.

[24] M. Sriti, Performance evaluation of wind turbines for energy production in Morocco's coastal regions, Results in Eng. 10 (2021) 100215, https://doi.org/10.1016/j.rineng.2021.100215.

[25] F. Harrou, A. Dairi, A. Dorbane, Y. Sun, Enhancing wind power prediction with self-attentive variational autoencoders: a comparative study, Results in Eng.. 23 (2024) 102504, https://doi.org/10.1016/j.rineng.2024.102504.

[26] R.K. Chaulagain, L. Poudel, S. Maharjan, Design and experimental analysis of a new vertical ultra-low-head hydro turbine with the variation of outlet flow level on the head drop section of an open canal, Results in Eng.. 22 (2024) 102240, https://doi.org/10.1016/j.rineng.2024.102240.

[27] Y.F. Kusuma, A.P. Fuadi, B. Al Hakim, C. Sasmito, A.C.P.T. Nugroho, M. H. Khoirudin, A.R. Prabowo, Navigating challenges on the path to net zero emissions: a comprehensive review of wind turbine technology for implementation in Indonesia, Results in Eng.. (2024) 102008, https://doi.org/10.1016/j.rineng.2024.102008.

[28] H. Seifi Davari, H. Chowdhury, M. Seify Davari, H. Hosseinzadeh, Optimizing airfoil efficiency for offshore turbines through aerodynamic geometry enhancement, Math. Anal. Contemp. Appl. 6 (1) (2024) 69–93, https://doi.org/10.30495/maca.2024.2017221.1092.

[29] H. Seifi Davari, M. Seify Davari, S. Kouravand, M. Kafili Kurdkandi, Optimizing the aerodynamic efficiency of different airfoils by altering their geometry at low Reynolds numbers, Arab, J. Sci. Eng. (2024) 1–36, https://doi.org/10.1007/s13369-024-08944-4.

[30] A. Alkhalidi, H. Kaylani, N. Alawawdeh, Technology assessment of offshore wind turbines: floating platforms–validated by case study, Results in Eng.. 17 (2023) 100831, https://doi.org/10.1016/j.rineng.2022.100831.

[31] H. Seifi Davari, M. Seifi Davary, S. Kouravand, Design of offshore vertical axis wind turbine with porous blades, J. Renew. New Energy 11 (2) (2024) 166–175, https://doi.org/10.22034/jrenew.2023.185089.

[32] P. Shakya, M. Thomas, A.C. Seibi, M. Shekaramiz, M.S. Masoum, Fluid-structure interaction and life prediction of small-scale damaged horizontal axis wind turbine blades, Results in Eng.. 23 (2024) 102388, https://doi.org/10.1016/j.rineng.2024.102388.

[33] H. Seifi Davari, M. Seify Davari, R. Botez, H. Chowdhury, Maximizing the peak lift-to-drag coefficient ratio of airfoils by optimizing the ratio of thickness to the camber of airfoils, Sustain. Earth Trends 3 (4) (2023) 46–61, https://doi.org/10.48308/ser.2024.234811.1036.

[34] W.A. Eltayeb, J. Somlal, S. Kumar, S.K. Rao, Design and analysis of a solar-wind hybrid renewable energy tree, Results in Eng.. 17 (2023) 100958, https://doi.org/10.1016/j.rineng.2023.100958.

[35] H.S. Davari, M.S. Davari, H. Chowdhury, R.M. Botez, Refining airfoil designs: tailored modifications for enhanced performance in low Reynolds number conditions, Sustain. Earth Rev. 4 (2) (2024), https://doi.org/10.48308/set.2024.235573.1050.

[36] A. Pujana-Arrese, I. Elorza, I. Trojaola, I. Arrizabalaga, E. Irigoyen, On the effects of pitch system faults on a wind turbine, Results in Eng.. 22 (2024) 102230, https://doi.org/10.1016/j.rineng.2024.102230.

[37] M.M. Kamal, A. Abbas, T. Alam, N.K. Gupta, R. Khargotra, Hybrid cross-flow hydrokinetic turbine: computational analysis for performance characteristics with helical Savonius blade angle of 135°, Results in Eng.. 20 (2023) 101610 https://doi.org/10.1016/j.rineng.2023.101610.

[38] K.A. Ismail, F.A. Lino, O. de Almeida, M. Teggar, V.L. Scalon, W.M. Okita, Review on small horizontal-axis wind turbines, Arab, J. Sci. Eng. 49 (2) (2024) 1367–1391, https://doi.org/10.1007/s13369-023-08314-6.

[39] H.A. Porto, C.A. Fortulan, A.V. Porto, Power performance of starting-improved and multi-bladed horizontal-axis small wind turbines, Sustain. Energy Technol. Assess. 53 (2022) 102341, https://doi.org/10.1016/j.seta.2022.102341.

[40] M.S.M. Shamsuddin, N.M. Kamaruddin, Experimental study on the characterization of the self-starting capability of a single and double-stage Savonius turbine, Results in Eng. 17 (2023) 100854, https://doi.org/10.1016/j.rineng.2022.100854.

[41] M.M. Peiravi, A. Ashabi, Hybrid investigation of the helical blades of Savonius wind turbine in novel patent of lighting base, Results in Eng. 15 (2022) 100565, https://doi.org/10.1016/j.rineng.2022.100565.

[42] M.H. Pranta, M.S. Rabbi, M.M. Roshid, A computational study on the aerodynamic performance of modified Savonius wind turbine, Results in Eng. 10 (2021) 100237, https://doi.org/10.1016/j.rineng.2021.100237.

[43] D. Gemayel, M. Abdelwahab, T. Ghazal, H. Aboshosha, Modelling of vertical axis wind turbine using large eddy simulations, Results in Eng. 18 (2023) 101226, https://doi.org/10.1016/j.rineng.2023.101226.

[44] H. Seifi Davari, S. Kouravand, M. Seify Davari, Z. Kamalnejad, Numerical investigation and aerodynamic simulation of Darrieus H-rotor wind turbine at low Reynolds numbers, Energy Sources, Part A: recovery, Utilization, Environ. Effects 45 (3) (2023) 6813–6833, https://doi.org/10.1080/15567036.2023.2213670.

[45] T. Wilberforce, A. Alaswad, Performance analysis of a vertical axis wind turbine using computational fluid dynamics, Energy 263 (2023) 125892, https://doi.org/10.1016/j.energy.2022.125892.

[46] H. Huang, J. Li, G. Li, Improving the self-starting and operating characteristics of vertical axis wind turbine by changing center distance in part of blades, J. Build. Eng. 68 (2023) 105974, https://doi.org/10.1016/j.jobe.2023.105974.

[47] S. Bhuyan, A. Biswas, Investigations on self-starting and performance characteristics of simple H and hybrid H-Savonius vertical axis wind rotors, Energy Convers. Manage 87 (2014) 859–867, https://doi.org/10.1016/j.enconman.2014.07.056.

[48] R. Dominy, P. Lunt, A. Bickerdyke, J. Dominy, Self-starting capability of a Darrieus turbine, Proc. Inst. Mech. Eng. Part A: J. Power Energy 221 (1) (2007) 111–120, https://doi.org/10.1243/09576509JPE340.

[49] Z. Sefidgar, A. Ahmadi Joneidi, A. Arabkoohsar, A comprehensive review on development and applications of cross-flow wind turbines, Sustainability. 15 (5) (2023) 4679, https://doi.org/10.3390/su15054679.

[50] K.A. Sunny, P. Kumar, N.M. Kumar, Experimental study on novel curved blade vertical axis wind turbines, Results in Eng. 7 (2020) 100149, https://doi.org/10.1016/j.rineng.2020.100149.

[51] P.F. Melani, F. Balduzzi, G. Ferrara, A. Bianchini, Development of a desmodromic variable pitch system for hydrokinetic turbines, Energy Convers. Manage. 250 (2021) 114890, https://doi.org/10.1016/j.enconman.2021.114890.

[52] A. Hosseini, N. Goudarzi, Design and CFD study of a hybrid vertical-axis wind turbine by employing a combined Bach-type and H-Darrieus rotor systems, Energy Convers. Manage. 189 (2019) 49–59, https://doi.org/10.1016/j.enconman.2019.03.068.

[53] M. Ahmad, A. Shahzad, F. Akram, F. Ahmad, S.I.A. Shah, Design optimization of Double-Darrieus hybrid vertical axis wind turbine, Ocean Eng 254 (2022) 111171, https://doi.org/10.1016/j.oceaneng.2022.111171.

[54] D. Sarkar, A.R. Sengupta, P. Bhadra, S. Alam, B. Debnath, Review of the Hybrid H-Savonius Rotor's Design and Performance, in: Recent Advances in Mechanical Engineering: Select Proceedings of ICRAME 2020, Springer, Singapore, 2021, pp. 33–40, https://doi.org/10.1007/978-981-15-7711-6_4.

[55] B. Cheng, Y. Yao, Design and optimization of a novel U-type vertical axis wind turbine with response surface and machine learning methodology, Energy Convers. Manage. 273 (2022) 116409, https://doi.org/10.1016/j.enconman.2022.116409.

[56] J. Su, Y. Chen, Z. Han, D. Zhou, Y. Bao, Y. Zhao, Investigation of V-shaped blade for the performance improvement of vertical axis wind turbines, Appl. Energy 260 (2020) 114326, https://doi.org/10.1016/j.apenergy.2019.114326.

[57] M. Zamani, S. Nazari, S.A. Moshizi, M.J. Maghrebi, Three dimensional simulation of J-shaped Darrieus vertical axis wind turbine, Energy 116 (2016) 1243–1255, https://doi.org/10.1016/j.energy.2016.10.031.

[58] Q. Liu, W. Miao, Q. Ye, C. Li, Performance assessment of an innovative Gurney flap for straight-bladed vertical axis wind turbine, Renew. Energy 185 (2022) 1124–1138, https://doi.org/10.1016/j.renene.2020.11.027.

[59] Y. Li, S. Zhao, K. Tagawa, F. Feng, Starting performance effect of a truncated-cone-shaped wind gathering device on small-scale straight-bladed vertical axis wind turbine, Energy Convers. Manage. 167 (2018) 70–80, https://doi.org/10.1016/j.enconman.2018.04.062.

[60] Y. Celik, L. Ma, D. Ingham, M. Pourkashanian, Aerodynamic investigation of the start-up process of H-type vertical axis wind turbines using CFD, J. Wind Eng. Ind. Aerodyn. 204 (2020) 104252, https://doi.org/10.1016/j.jweia.2020.104252.

[61] S.Y. Sun, H.J. Liu, H.Y. Peng, Power performance and self-starting features of H-rotor and helical vertical axis wind turbines with different airfoils in turbulence, Energy Convers. Manage. 292 (2023) 117405, https://doi.org/10.1016/j.enconman.2023.117405.

[62] L. Battisti, A. Brighenti, E. Benini, M.R. Castelli, Analysis of different blade architectures on small VAWT performance, J. Phys. Conf. Ser. 753 (2016) 062009, https://doi.org/10.1088/1742-6596/753/6/062009.

[63] T. Maeda, Y. Kamada, J. Murata, K. Furukawa, M. Yamamoto, Effect of number of blades on aerodynamic forces on a straight-bladed Vertical Axis Wind Turbine, Energy 90 (2015) 784–795, https://doi.org/10.1016/j.energy.2015.07.115.

[64] C. Simão Ferreira, G. Van Kuik, G. Van Bussel, F. Scarano, Visualization by PIV of dynamic stall on a vertical axis wind turbine, Exp. Fluids 46 (2009) 97–108, https://doi.org/10.1007/s00348-008-0543-z.

[65] B. Hand, G. Kelly, A. Cashman, Numerical simulation of a vertical axis wind turbine airfoil experiencing dynamic stall at high Reynolds numbers, Comput. Fluids 149 (2017) 12–30, https://doi.org/10.1016/j.compfluid.2017.02.021.

[66] K. Mulleners, M. Raffel, The onset of dynamic stall revisited, Exp. Fluids 52 (2012) 779–793, https://doi.org/10.1007/s00348-011-1118-y.

[67] A. Rezaeiha, H. Montazeri, B. Blocken, CFD analysis of dynamic stall on vertical axis wind turbines using Scale-Adaptive Simulation (SAS): comparison against URANS and hybrid RANS/LES, Energy Convers. Manage. 196 (2019) 1282–1298, https://doi.org/10.1016/j.enconman.2019.06.081.

[68] A. Rezaeiha, H. Montazeri, B. Blocken, CFD investigation of separation control on a vertical axis wind turbine: steady and unsteady suction, J. Phys. Conf. Ser. 1618 (2020) 052019, https://doi.org/10.1088/1742-6596/1618/5/052019.

[69] M.R. Tirandaz, A. Rezaeiha, Effect of airfoil shape on power performance of vertical axis wind turbines in dynamic stall: symmetric Airfoils, Renew. Energy 173 (2021) 422–441, https://doi.org/10.1016/j.renene.2021.03.142.

[70] K.Y. Lee, A. Cruden, J.H. Ng, K.H. Wong, Variable designs of vertical axis wind turbines—A review, Front. Energy Res. 12 (2024) 1437800, https://doi.org/10.3389/fenrg.2024.1437800.

[71] S.D. Karmakar, H. Chattopadhyay, A review of augmentation methods to enhance the performance of vertical axis wind turbine, Sustain. Energy Technol. Assess. 53 (2022) 102469, https://doi.org/10.1016/j.seta.2022.102469.

[72] D. Zhou, D. Zhou, Y. Xu, X. Sun, Performance enhancement of straight-bladed vertical axis wind turbines via active flow control strategies: a review, Meccanica (2022) 1–28, https://doi.org/10.1007/s11012-021-01445-w.

[73] A.H. Rajpar, I. Ali, A.E. Eladwi, M.B.A. Bashir, Recent development in the design of wind deflectors for vertical axis wind turbine: a review, Energies. (Basel) 14 (16) (2021) 5140, https://doi.org/10.3390/en14165140.

[74] H.Y. Peng, H.F. Lam, H.J. Liu, Power performance assessment of H-rotor vertical axis wind turbines with different aspect ratios in turbulent flows via experiments, Energy 173 (2019) 121–132, https://doi.org/10.1016/j.energy.2019.01.140.

[75] Y.K. Wu, H.J. Lin, J.H. Lin, Certification and testing technology for small vertical axis wind turbine in Taiwan, Sustain. Energy Technol. Assess. 31 (2019) 34–42, https://doi.org/10.1016/j.seta.2018.11.005.

[76] W.C. Wang, J.J. Wang, W.T. Chong, The effects of unsteady wind on the performances of a newly developed cross-axis wind turbine: a wind tunnel study, Renew. Energy 131 (2019) 644–659, https://doi.org/10.1016/j.renene.2018.07.061.

[77] M. Al-Ghriybah, M.F. Zulkafli, D.H. Didane, S. Mohd, The effect of inner blade position on the performance of the Savonius rotor, Sustain. Energy Technol. Assess. 36 (2019) 100534, https://doi.org/10.1016/j.seta.2019.100534.

[78] N. Franchina, G. Persico, M. Savini, 2D-3D computations of a vertical axis wind turbine flow field: modeling issues and physical interpretations, Renew. Energy 136 (2019) 1170–1189, https://doi.org/10.1016/j.renene.2018.09.086.

[79] G. Bedon, M.R. Castelli, E. Benini, Proposal for an innovative chord distribution in the Troposkien vertical axis wind turbine concept, Energy 66 (2014) 689–698, https://doi.org/10.1016/j.energy.2014.01.004.

[80] F. Balduzzi, J. Drofelnik, A. Bianchini, G. Ferrara, L. Ferrari, M.S. Campobasso, Darrieus wind turbine blade unsteady aerodynamics: a three-dimensional Navier-Stokes CFD assessment, Energy 128 (2017) 550–563, https://doi.org/10.1016/j.energy.2017.04.017.

[81] Y.X. Peng, Y.L. Xu, S. Zhan, A hybrid DMST model for pitch optimization and performance assessment of high-solidity straight-bladed vertical axis wind turbines, Appl. Energy 250 (2019) 215–228, https://doi.org/10.1016/j.apenergy.2019.04.127.

[82] G. Bangga, A. Dessoky, T. Lutz, E. Krämer, Improved double-multiple-streamtube approach for H-Darrieus vertical axis wind turbine computations, Energy 182 (2019) 673–688, https://doi.org/10.1016/j.energy.2019.06.083.

[83] M. Tahani, N. Babayan, S. Mehrnia, M. Shadmehri, A novel heuristic method for optimization of straight blade vertical axis wind turbine, Energy Convers. Manage. 127 (2016) 461–476, https://doi.org/10.1016/j.enconman.2016.08.094.

[84] M. Moghimi, H. Motawej, Developed DMST model for performance analysis and parametric evaluation of Gorlov vertical axis wind turbines, Sustain. Energy Technol. Assess. 37 (2020) 100616, https://doi.org/10.1016/j.seta.2019.100616.

[85] N.C. Batista, R. Melício, V.M.F. Mendes, M. Calderón, A. Ramiro, On a self-start Darrieus wind turbine: blade design and field tests, Renew. Sustain. Energy Rev. 52 (2015) 508–522, https://doi.org/10.1016/j.rser.2015.07.147.

[86] M. Islam, Analysis of fixed-pitch straight-bladed VAWT with asymmetric airfoils (2008).

[87] I. Paraschivoiu, Wind Turbine design: With Emphasis On Darrieus concept, Presses inter Polytechnique, 2002.

[88] P. Ghiasi, G. Najafi, B. Ghobadian, A. Jafari, M. Mazlan, Analytical study of the impact of solidity, chord length, number of blades, aspect ratio and airfoil type on h-rotor Darrieus wind turbine performance at low Reynolds number, Sustainability. 14 (5) (2022) 2623, https://doi.org/10.3390/su14052623.

[89] M. Elkhoury, T. Kiwata, E. Aoun, Experimental and numerical investigation of a three-dimensional vertical-axis wind turbine with variable-pitch, J. Wind Eng. Ind. Aerodyn. 139 (2015) 111–123, https://doi.org/10.1016/j.jweia.2015.01.004.

[90] S.C. Roh, S.H. Kang, Effects of a blade profile, the Reynolds number, and the solidity on the performance of a straight bladed vertical axis wind turbine, J. Mech. Sci. Technol. 27 (11) (2013) 3299–3307, https://doi.org/10.1007/s12206-013-0852-x.

[91] Y.X. Peng, Y.L. Xu, S. Zhu, C. Li, High-solidity straight-bladed vertical axis wind turbine: numerical simulation and validation, J. Wind Eng. Ind. Aerodyn. 193 (2019) 103960, https://doi.org/10.1016/j.jweia.2019.103960.

[92] J. Guo, P. Zeng, L. Lei, Performance of a straight-bladed vertical axis wind turbine with inclined pitch axes by wind tunnel experiments, Energy 174 (2019) 553–561, https://doi.org/10.1016/j.energy.2019.02.177.

[93] T. Maeda, Y. Kamada, J. Murata, K. Shimizu, T. Ogasawara, A. Nakai, T. Kasuya, Effect of solidity on aerodynamic forces around straight-bladed vertical axis wind turbine by wind tunnel experiments (depending on number of blades), Renew. Energy 96 (2016) 928–939, https://doi.org/10.1016/j.renene.2016.05.054.

[94] W. Guo, H. Shen, Y. Li, F. Feng, K. Tagawa, Wind tunnel tests of the rime icing characteristics of a straight-bladed vertical axis wind turbine, Renew. Energy 179 (2021) 116–132, https://doi.org/10.1016/j.renene.2021.07.033.

[95] Y. Li, K. Tagawa, W. Liu, Performance effects of attachment on blade on a straight-bladed vertical axis wind turbine, Curr. Appl. Phys. 10 (2) (2010) S335–S338, https://doi.org/10.1016/j.cap.2009.11.072.

[96] W.C. Wang, W.T. Chong, T.H. Chao, Performance analysis of a cross-axis wind turbine from wind tunnel experiments, J. Wind Eng. Ind. Aerodyn. 174 (2018) 312–329, https://doi.org/10.1016/j.jweia.2018.01.023.

[97] Y.L. Xu, Y.X. Peng, S. Zhan, Optimal blade pitch function and control device for high-solidity straight-bladed vertical axis wind turbines, Appl. Energy 242 (2019) 1613–1625, https://doi.org/10.1016/j.apenergy.2019.03.151.

[98] A.R. Sengupta, A. Biswas, R. Gupta, Studies of some high solidity symmetrical and unsymmetrical blade H-Darrieus rotors with respect to starting characteristics, dynamic performances and flow physics in low wind streams, Renew. Energy 93 (2016) 536–547, https://doi.org/10.1016/j.renene.2016.03.029.

[99] R. Gosselin, G. Dumas, M. Boudreau, Parametric study of H-Darrieus vertical-axis turbines using CFD simulations, J. Renew. Sustain. Energy 8 (2016) 053301, https://doi.org/10.1063/1.4963240.

[100] R. Espina-Valdés, A. Fernández-Jiménez, J.F. Francos, E.B. Marigorta, E. Álvarez-Álvarez, Small cross-flow turbine: design and testing in high blockage conditions, Energy Convers. Manage. 213 (2020) 112863, https://doi.org/10.1016/j.enconman.2020.112863.

[101] Y. Zhang, Z. Guo, X. Zhu, Y. Li, X. Song, C. Cai, T. Maeda, Investigation of aerodynamic forces and flow field of an H-type vertical axis wind turbine based on bionic airfoil, Energy 242 (2022) 122999, https://doi.org/10.1016/j.energy.2021.122999.

[102] M.S. Abul-Ela, A.I. Sayed, M.E.F. Elrefaei, Performance comparative study of low Reynolds number airfoils utilized in vertical-axis wind turbines, J. Al-Azhar Uni. Eng. Sector 19 (72) (2024) 147–161, https://doi.org/10.21608/auej.2024.257724.1548.

[103] B. Abotaleb, M.M. Takeyeldein, O. Huzayyin, B. Elhadidi, Impact of negative camber for performance of vertical axis wind turbine, (2024), https://doi.org/10.5109/7172281.

[104] M.Ö. Korukçu, Impact of blade modifications on the performance of a Darrieus wind turbine, Processes 12 (4) (2024) 732, https://doi.org/10.3390/pr12040732.

[105] K. Kord, M. Bazargan, Numerical Investigation on J-Shaped Straight-Bladed Darrieus Vertical Axis Wind Turbines Equipped with Gurney Flaps, Int. J. Energy Res. 1 (2024) 8992210, https://doi.org/10.1155/2024/8992210.

[106] G.M. Avalos, N.R. Hau, R. Quintal-Palomo, E.O. López, M. Gamboa-Marrufo, M. E. Soberanis, Aerodynamic techniques to mitigate the 3D loss in the power coefficient of vertical axis wind turbines, Energy Convers. Manage. 311 (2024) 118507, https://doi.org/10.1016/j.enconman.2024.118507.

[107] W.U. Hassan, A. Jalal, M.A. Bilal, M.Z. Buzal, H. Asghar, U. Ali, Parametric analysis of a helical-bladed vertical axis wind turbine, J. Ocean Eng. Mar. Energy 10 (2) (2024) 383–398, https://doi.org/10.1007/s40722-024-00318-0.

[108] K.U. Reddy, B. Deb, B. Roy, Experimental study on influence of aspect ratio and auxiliary blade profile on the performance of H-Type Darrieus wind rotor, Arab,

J. Sci. Eng. 49 (2) (2024) 1913–1929, https://doi.org/10.1007/s13369-023-08049-4.
[109] H.E. Tanürün, A.G. Akın, A. Acır, İ. Şahin, Experimental and Numerical Investigation of Roughness Structure in Wind Turbine Airfoil at Low Reynolds Number, Int. J. Thermodyn. 27 (3) (2024) 26–36, https://doi.org/10.5541/ijot.1455513.
[110] K. Pietrykowski, N. Kasianantham, D. Ravi, M.J. Gęca, P. Ramakrishnan, M. Wendeker, Sustainable energy development technique of vertical axis wind turbine with variable swept area–An experimental investigation, Appl. Energy 329 (2023) 120262, https://doi.org/10.1016/j.apenergy.2022.120262.
[111] M.E. Nimvari, H. Fatahian, E. Fatahian, Performance improvement of a Savonius vertical axis wind turbine using a porous deflector, Energy Convers. Manage. 220 (2020) 113062, https://doi.org/10.1016/j.enconman.2020.113062.
[112] M. Somoano, F.J. Huera-Huarte, Bio-inspired blades with local trailing edge flexibility increase the efficiency of vertical axis wind turbines, Energy Rep. 8 (2022) 3244–3250, https://doi.org/10.1016/j.egyr.2022.02.151.
[113] I. Basker, M.Nainangkuppam Venkatesan, 3D-CFD flow driven performance analysis of new non-cylindrical helical vertical axis wind turbine for fluctuating urban wind conditions, energy sources, part A: recovery, Utiliz. Environ. Effects 44 (1) (2022) 2186–2207, https://doi.org/10.1080/15567036.2022.2058654.
[114] S. Mitchell, I. Ogbonna, K. Volkov, Improvement of self-starting capabilities of vertical axis wind turbines with new design of turbine blades, Sustainability. 13 (7) (2021) 3854, https://doi.org/10.3390/su13073854.
[115] H. Chang, D. Li, R. Zhang, H. Wang, Y. He, Z. Zuo, S. Liu, Effect of discontinuous biomimetic leading-edge protuberances on the performance of vertical axis wind turbines, Appl. Energy 364 (2024) 123117, https://doi.org/10.1016/j.apenergy.2024.123117.
[116] D.W. MacPhee, A. Beyene, Fluid–structure interaction analysis of a morphing vertical axis wind turbine, J. Fluids Struct. 60 (2016) 143–159, https://doi.org/10.1016/j.jfluidstructs.2015.10.010.
[117] W. Guo, S. Gong, Z. Shen, Y. Gong, H. Lu, Effects of internal rotor parameters on the performance of curved blade-straight blade vertical axis wind turbine, Energy Convers. Manag. 321 (2024) 119078, https://doi.org/10.1016/j.enconman.2024.119078.
[118] T.P. Syawitri, Y. Yao, J. Yao, B. Chandra, Geometry optimisation of vertical axis wind turbine with Gurney flap for performance enhancement at low, medium, and high ranges of tip speed ratios, Sustain. Energy Technol. Assess. 49 (2022) 101779, https://doi.org/10.1016/j.jweia.2024.105853.
[119] H. Seifi, S. Kouravand, M.S. Davary, S. Mohammadzadeh, Numerical and experimental study of the effect of increasing aspect ratio of self-starting force to vertical axis wind turbine, J. Renew. New Energy 10 (1) (2023) 1–14, https://doi.org/10.52547/jrenew.10.1.1.
[120] H. Seifi, S. Kouravand, M. Seifi Davary, Numerical and experimental study of NACA airfoil in low Reynolds numbers for use of Darrieus vertical axis micro-wind turbine, J. Renew. New Energy 10 (2) (2023) 149–163, https://doi.org/10.52547/jrenew.10.2.149.
[121] H. Seifi Davari, R.M. Botez, M. Seify Davari, H. Chowdhury, Enhancing the efficiency of horizontal axis wind turbines through optimization of blade parameters, J. Eng. 8574868 (2024), https://doi.org/10.1155/2024/8574868.
[122] A.S. Nagaraju, R. Gupta, S. Bhowmik, Effects of the influence of triangular dimple and aspect ratio on NACA 4412 airfoil on the overall performance of H-Darrieus wind rotor: an experimental investigation, Wind Eng. (2024), https://doi.org/10.1177/0309524X241256955.
[123] H. Su, B. Dou, T. Qu, P. Zeng, L. Lei, Experimental investigation of a novel vertical axis wind turbine with pitching and self-starting function, Energy Convers. Manage. 217 (2020) 113012, https://doi.org/10.1016/j.enconman.2020.113012.
[124] R.K. Kavade, M.M. Sonekar, D.S. Choudhari, P.D. Malwe, N.P. Sherje, M. A. Ansari, A. Kumar, Investigation on fixed pitch Darrieus vertical axis wind turbine, AIP. Adv. 14 (7) (2024), https://doi.org/10.1063/5.0203609.
[125] Z. Xu, X. Dong, K. Li, Q. Zhou, Y. Zhao, Study of the self-starting performance of a vertical-axis wind turbine, J. Appl. Fluid Mech. 17 (6) (2024) 1261–1276, https://doi.org/10.47176/jafm.17.6.2295.
[126] H.M.S.M. Mazarbhuiya, A. Biswas, K.K. Sharma, Low wind speed aerodynamics of asymmetric blade H-Darrieus wind turbine-its desired blade pitch for performance improvement in the built environment, J. Braz. Soc. Mech. Sci. Eng. 42 (6) (2020) 326, https://doi.org/10.1007/s40430-020-02408-0.
[127] H.Y. Peng, X.R. Yang, H.J. Liu, S.Y. Sun, Aerodynamic analysis of vertical axis wind turbines at various turbulent levels: insights from 3D LES simulations, J. Build. Eng. 109899 (2024), https://doi.org/10.1016/j.jobe.2024.109899.
[128] H. Huang, J. Luo, G. Li, Study on the optimal design of vertical axis wind turbine with novel variable solidity type for self-starting capability and aerodynamic performance, Energy 271 (2023) 127031, https://doi.org/10.1016/j.energy.2023.127031.
[129] M. Zamani, A. Sangtarash, M.J. Maghrebi, Numerical study of porous media effect on the blade surface of vertical axis wind turbine for enhancement of aerodynamic performance, Energy Convers. Manage. 245 (2021) 114598, https://doi.org/10.1016/j.enconman.2021.114598.
[130] Y. Yang, Y. Cao, Z. Qian, J. Wang, Y. Zhu, X. Chen, S. Chen, A study on the effect of turbulence intensity on dual vertical-axis wind turbine aerodynamic performance, Energies. (Basel) 17 (16) (2024) 4124, https://doi.org/10.3390/en17164124.
[131] M. Ahmad, A. Shahzad, F. Akram, M.N.M. Qadri, Determination of efficient configurations of vertical axis wind turbine using design of experiments, Proc. Inst. Mech. Eng. A: J. Power Energy 236 (8) (2022) 1558–1581, https://doi.org/10.1177/09576509221095347.
[132] M.S.U. Khalid, D. Wood, A. Hemmati, Self-starting characteristics and flow-induced rotation of single- and dual-stage vertical-axis wind turbines, Energies. (Basel) 15 (24) (2022) 9365, https://doi.org/10.3390/en15249365.
[133] M.S.M. Ghareghani, A. Abdolahifar, S. Karimian, Numerical investigation on the heliX angle to smoothen aerodynamic torque output of the 3-PB Darrieus vertical axis wind turbine, J. Wind Eng. Ind. Aerod. 234 (2023) 105323, https://doi.org/10.1016/j.jweia.2023.105323.
[134] X. Sun, J. Zhu, Z. Li, G. Sun, Rotation improvement of vertical axis wind turbine by offsetting pitching angles and changing blade numbers, Energy 215 (2021) 119177, https://doi.org/10.1016/j.energy.2020.119177.